Vibrational frequency shift of HF in helium clusters: Quantum simulation and experiment

Dörte Blume, Marius Lewerenz, Friedrich Huisken, and Michael Kaloudis

Citation: The Journal of Chemical Physics **105**, 8666 (1996); doi: 10.1063/1.472648
View online: http://dx.doi.org/10.1063/1.472648
View Table of Contents: http://scitation.aip.org/content/aip/journal/jcp/105/19?ver=pdfcov
Published by the AIP Publishing

Vibrational frequency shift of HF in helium clusters: Quantum simulation and experiment

Dörte Blume, Marius Lewerenz, Friedrich Huisken, and Michael Kaloudis
Max-Planck-Institut für Strömungsforschung, Bunsenstrasse 10, 37073 Göttingen, Germany

(Received 18 April 1996; accepted 15 August 1996)

We report accurate variational and diffusion quantum Monte Carlo calculations for the size dependence of the vibrational frequency shift of HF molecules embedded in helium clusters with up to $n=198$ helium atoms. The frequency shift exhibits a strong initial size dependence and saturates at a redshift of about 2.7 ± 0.1 cm^{-1} for clusters with over 100 atoms. This value is in good agreement with our experimental redshift of 2.65 ± 0.15 cm^{-1} for clusters with over 1000 atoms. The helium cluster is found to undergo significant structural changes upon embedding of HF. The density in the nearest neighbor shell exceeds the bulk helium density by a factor of two. A second nearest neighbor density maximum and a peripheral density plateau very close to the bulk helium value is found. In spite of the anisotropic interaction between HF and helium all clusters have almost perfectly spherical helium density profiles and indicate close to free rotor behavior of HF inside the cluster. The cluster size dependence of the redshift can be qualitatively described by an induced dipole model. © *1996 American Institute of Physics.* [S0021-9606(96)02243-X]

I. INTRODUCTION

The study of the structure of quantum clusters has evolved into a rather active field in recent years. Originally dominated by theoretical studies on pure helium and hydrogen clusters[1–5] the field has profited greatly from a number of recent scattering[6–8] and spectroscopic studies of clusters with embedded probe molecules.[9–12] These spectroscopic experiments were invariably carried out on clusters with several hundred to several thousand atoms. At the other end of the size range we find only a few spectroscopic studies of small van der Waals complexes.[13,14] There has been considerable recent theoretical interest in the structure and energetics of quantum clusters with impurities.[3,15–17] However only few theoretical studies have attempted to calculate measurable spectroscopic properties of quantum clusters with molecular impurities for cluster sizes which allow direct comparison with experimental data. The calculation of Barnett and Whaley[18] for SF_6 in helium clusters was a vibrational ground state quantum simulation employing a perturbational estimate of the vibrational frequency shift based on the induced dipole model of Eichenauer and Leroy[19] and gave a redshift of about 0.9 cm^{-1} for the ν_3 vibration of SF_6 in large helium clusters which differs noticeably from the observed value of about 1.4 cm^{-1}.[11]

The main spectroscopic observables are the shift of the vibrational or electronic excitation[10,12,20] of the embedded molecule and the rotational or vibrotational fine structure of these bands which provide insight into the interaction between the quantum matrix and the molecular probe. Recent data on the electronic excitation of glyoxal[12] have been interpreted as evidence for superfluid behavior of helium clusters with a few thousand atoms and emphasize the need for a microscopic understanding of the spectroscopic signatures of molecules embedded in quantum liquids.

In this paper we want to demonstrate the ability of advanced quantum theoretical methods to make quantitative predictions for vibrational frequency shifts and to answer questions regarding the structural perturbation of the quantum cluster by the probe molecule and the perturbation of the molecule due to the interaction with the quantum liquid bath. A related question is: When is a cluster ''large'' in the sense that the perturbation by the probe does not affect the periphery of the cluster and further increase of the cluster size does not change the spectroscopic signature of the probe? This size would define the bulk matrix limit for this particular property. The evolution of these properties in the transition from small van der Waals complexes to a solvated molecule[21] is another piece of information which can be extracted from the calculations. Corresponding experiments on size selected helium clusters have now become possible in principle[7,22] but no attempts at spectroscopic studies have been undertaken yet.

Helium clusters with embedded HF provide an interesting test case for theoretical methods. There are several potential surfaces for the van der Waals complex HeHF extracted from experimental information[23,24] or based on *ab initio* calculations.[25] The helium–helium pairwise interaction is sufficiently well characterized[26,27] to allow the construction of a reasonable pairwise additive surface for a large cluster. Since three body terms are known to be rather small for helium,[28] this additive model is also expected to be a good approximation to the real cluster thereby allowing meaningful comparisons between calculated data and experimental results. The accuracy of our method for the solution of the many body Schrödinger equation can be tested against high quality variational calculations which are possible for the binary complex HeHF.[24,29,30] From an experimental point of view HF is a good candidate because of its strong infrared absorption and simple spectrum and the absence of isotopic congestion.

In Sec. II of the paper we will explain the computational methods employed to provide an accurate solution of the

many body Schrödinger equation and special developments for the calculation of small perturbations. Section III describes the experimental setup used to record vibrational spectra of molecules embedded in helium clusters using a depletion technique in combination with a tunable infrared light source. Finally we compare and discuss the results of calculations and experiments carried out on the system He_nHF in Sec. IV.

II. COMPUTATIONAL METHODS

The only methods available for an accurate treatment of quantum systems with very many degrees of freedom are based on stochastic approaches and are collectively referred to as quantum Monte Carlo.[31–35] Their main advantages are the absence of system size dependent errors which allows unbiased computations of size dependent properties[36–38] and the favorable scaling of the computational effort with the number of degrees of freedom. These methods are particularly suited to the treatment of very floppy systems where quantum mechanical mixing of several classical structures is an important feature.

A practical advantage is the ability to employ a Hamiltonian formulated in Cartesian coordinates and to provide quantitative estimates of the accuracy achieved with a given calculation by statistical means. An often overlooked advantage of quantum Monte Carlo methods is the low storage requirement which grows only linearly with the number of particles and makes calculations on very large systems feasible on machines with relatively small memory. The alternative use of traditional basis set expansion methods turns out to be currently more limited by memory requirements than by computer speed. The inherent parallelism of the random walk methods described in the next paragraphs is perfectly suited for modern computer architectures and gives them great potential for the future.

Most quantum Monte Carlo methods are ground state methods. Calculations of frequency shifts are possible, however, in the framework of an adiabatic approximation. The high frequency motion of HF is a perfect candidate for adiabatic decoupling from the soft vibrational modes of the cluster. This separation scheme is at the heart of most potential surfaces constructed for molecular van der Waals complexes.[39] It is often the only available scheme because either the lack of experimental data or the impossibility of scanning a large number of coordinates in an *ab initio* treatment precludes the determination of complete surfaces.

In the following paragraphs we will explain the main features of the two quantum Monte Carlo methods used in the present work, namely variational quantum Monte Carlo (VMC) and diffusion quantum Monte Carlo (DMC) methods.

A. Variational quantum Monte Carlo method

Our first set of calculations was done using the variational quantum Monte Carlo method (VMC). It provides approximate solutions to complicated quantum problems at moderate cost and is of particular value in conjunction with the diffusion quantum Monte Carlo (DMC) method described later. The variational nature of the method provides an upper bound for the total energy. The key idea of the method is the construction of a trial wave function $\Psi_T(\vec{r};\vec{p})$ for which the energy expectation value is computed using a random walk based Monte Carlo quadrature. The energy is subsequently minimized by adjustment of parameters $\vec{p}$ controlling the shape of the trial wave function

$$E_{\text{exact}} \leqslant E(\vec{p}) = \frac{\int \Psi_T^*(\vec{r};\vec{p}) \hat{H} \Psi_T(\vec{r};\vec{p}) d\vec{r}}{\int |\Psi_T(\vec{r};\vec{p})|^2 d\vec{r}}. \tag{1}$$

In the following we use Ψ_T whenever we refer to the total trial wave function, $\vec{r}$ stands for the collection of spatial coordinates of the particles, $\vec{p}$ denotes the set of adjustable parameters controlling the trial wave function, and $\hat{H}$ is the Hamiltonian of the system which may be expressed in arbitrary coordinates.

Equation (1) can be recast into an integral over the product of a normalized weight function and a residual function according to

$$E(\vec{p}) = \frac{\int |\Psi_T(\vec{r};\vec{p})|^2 \Psi_T^{-1}(\vec{r};\vec{p}) \hat{H} \Psi_T(\vec{r};\vec{p}) d\vec{r}}{\int |\Psi_T(\vec{r};\vec{p})|^2 d\vec{r}}. \tag{2}$$

This type of integral can be easily and efficiently evaluated by Monte Carlo techniques which replace the integral by a finite sum over a set of random samples $\vec{r}_i$ drawn from the normalized probability density function $|\Psi_T(\vec{r};\vec{p})|^2 / \int |\Psi_T(\vec{r};\vec{p})|^2 d\vec{r}$[40]

$$E(\vec{p}) \approx \langle E(\vec{p}) \rangle = \frac{1}{N} \sum_{i=1}^{N} \Psi_T^{-1}(\vec{r}_i;\vec{p}) \hat{H} \Psi_T(\vec{r}_i;\vec{p}). \tag{3}$$

We use the standard method for the generation of samples in multidimensional spaces namely a Metropolis random walk.[41] The main quantity of interest is the ''local energy''

$$\begin{aligned} E_{\text{local}}(\vec{r};\vec{p}) &= \Psi_T^{-1}(\vec{r};\vec{p}) \hat{H} \Psi_T(\vec{r};\vec{p}) \\ &= \Psi_T^{-1}(\vec{r};\vec{p}) \hat{T} \Psi_T(\vec{r};\vec{p}) + V(\vec{r}), \end{aligned} \tag{4}$$

which is averaged to obtain the statistical estimate of the energy expectation value. The occurrence of Ψ_T^{-1} in this expression does not impose any restrictions on the trial wave functions since the sampling density $|\Psi_T|^2$ is zero at nodal positions where the local energy would diverge.

Besides the minimization of the energy $E(\vec{p})$ with respect to all parameters we employ simultaneous minimization of its variance to obtain the best wave function Ψ_T within the limits of a given functional form.[42] The variance approaches zero as the wave function $\Psi_T(\vec{p})$ approaches the exact wave function Ψ since in this limit the local energy is identical to the eigenvalue, irrespective of $\vec{r}$. While the energy minimization emphasizes global correctness of Ψ_T, the variance $\text{Var}\{E\}$ is sensitive to local errors in Ψ_T. We minimize both quantities using a combination of coarse manual variation of parameters and conjugate gradient minimization

for the final refinement. For the accurate determination of the proper downhill direction we use the technique of reweighting[31] to create correlated energy samples at neighboring points in parameter space and finite differencing.

The main limitation of the VMC method goes back to the choice of the functional form for Ψ_T which requires special care and good insight into the physics of the system being treated. A common ansatz for atomic clusters and bulk systems[31] expresses Ψ_T as a product over a set of one-dimensional functions Φ defined over all pairs of particles

$$\Psi_T(\vec{r};\vec{p})=\prod_{i<j}\Phi_{ij}(r_{ij};\vec{p}), \tag{5}$$

where r_{ij} is the distance between particles i and j. For this type of trial wave function one can easily derive a convenient expression for the local energy which allows modular programming and the assembly of its value from derivatives of the component functions Φ:

$$\begin{aligned}\Psi_T^{-1}\hat{T}\Psi_T=-\sum_i\frac{\hbar^2}{2m_i}\Bigg\{\sum_{q=x,y,z}\Bigg[\sum_{j\neq i}\frac{1}{r_{ij}}\frac{\partial\ln\Phi_{ij}}{\partial r_{ij}}(q_i-q_j)\Bigg]^2\\+\sum_{j\neq i}\Bigg[\frac{2}{r_{ij}}\frac{\partial\ln\Phi_{ij}}{\partial r_{ij}}+\frac{1}{\Phi_{ij}}\frac{\partial^2\Phi_{ij}}{\partial r_{ij}^2}\\-\left(\frac{\partial\ln\Phi_{ij}}{\partial r_{ij}}\right)^2\Bigg]\Bigg\}.\end{aligned} \tag{6}$$

In our case of a diatomic molecule embedded in an atomic environment this approach has to be modified. In the following we will always use HF to denote the diatomic and He to refer to the rare gas atoms but the formalism (and our computer code) is valid for an arbitrary diatomic molecule embedded in a collection of equivalent atoms. Since the anisotropy of the interaction between the molecule and the surrounding rare gas atoms will generally be reflected in the shape of the wave function, this feature has to be built into the functional form in an appropriate way. We write Ψ_T as a product over pairwise radial functions Φ as above connecting the rare gas atoms and a product over anisotropic two-dimensional functions χ describing the anisotropic molecule–rare gas contribution:

$$\Psi_T(\vec{r};\vec{p})=\prod_{i\in\mathrm{He}}\chi_i(r_i,\theta_i;\vec{p})\cdot\prod_{i<j\in\mathrm{He}}\Phi_{ij}(r_{ij};\vec{p}). \tag{7}$$

The r_{ij} are distances between rare gas atoms i and j, and r_i,θ_i are Jacobi coordinates describing the distance between rare gas atom i and the center of mass of HF and the angle between the r_i vector and the HF bond vector. This form of Ψ_T satisfies the proper exchange symmetry for ^{4}He. There is no explicit dependence of Ψ_T on the HF distance since our current treatment assumes adiabatic separability between the molecular vibration and the intermolecular vibrations in agreement with previous treatments of small van der Waals complexes[39,43] and the structure of the available HeHF potential energy surface.[25] The inclusion of an additional molecular part for a nonadiabatic treatment is straightforward.

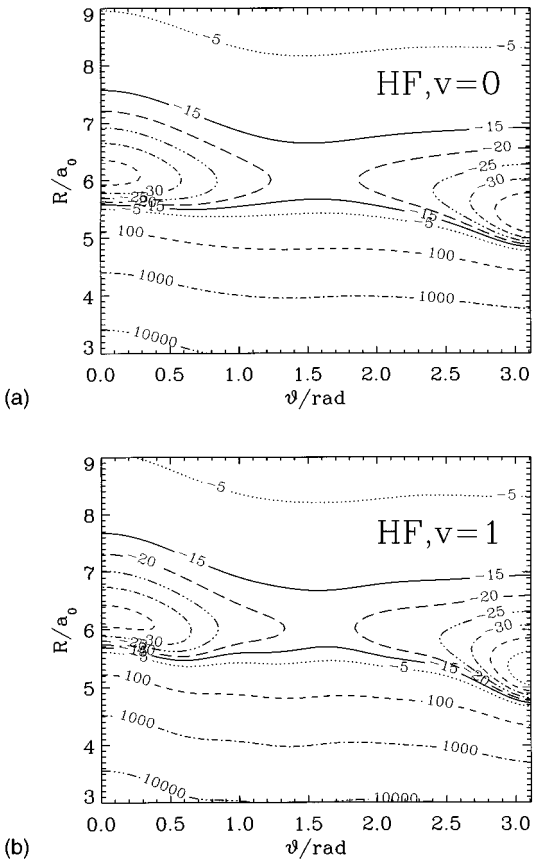

FIG. 1. Adiabatic potential energy surfaces for HeHF for HF in its vibrational ground state (top) and in its first excited state (bottom). R is the Jacobi distance between helium and the center of mass of HF, θ is the Jacobi angle. $\theta=0$ corresponds to the He$\cdots$HF arrangement. Contour levels are given in cm^{-1}.

Previous experience with helium clusters[42] showed that Jastrow functions are a good choice for Φ and were also employed in the present work. In order to minimize the number of parameters to be optimized we chose to describe the He–He part of the wave function by a purely repulsive edge. The cluster is held together by an attractive long range tail in the χ part of the wave function which is also of Jastrow form with angle dependent parameters describing the inner edge:

$$\begin{aligned}\Phi(r)&=\exp\left[-\ln 2\left(\frac{p_0}{r}\right)^5\right],\\ \chi^{(1)}(r,\theta)&=A(\theta;p_3)\exp\left[-\ln 2\left(\frac{p_1}{r}\right)^5 B(\theta;p_4)-p_2 r\right].\end{aligned} \tag{8}$$

The long range exponential decay of the wave function was taken as isotropic. The angle dependence of the parameters A and B controlling the amplitude of χ and the position of the inner repulsive edge was chosen according to the shape of the HeHF potential surface displayed in Fig. 1 for two different HF distances.

Its main qualitative features are two minima of similar depth at linear arrangements separated by a barrier close to $\theta=\pi/2$ and a difference in the Jacobi distance of the minima of the two wells. Details of the surface are discussed in Sec.

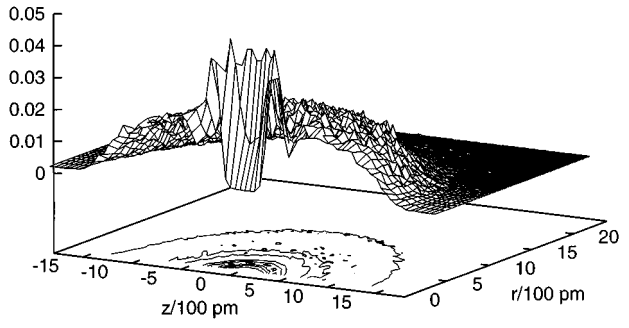

FIG. 2. Two-dimensional helium density in units of $Å^{-3}$ for $He_{198}HF$ computed with DMC and descendant weighting. Contour lines are at density levels of 0.01, 0.02, 0.03, and 0.04 $Å^{-3}$.

II F. The resulting effect on the overall shape of the wave function can be represented by Legendre polynomials of degree 2 and 1, respectively

$$A(\theta;p_3)=1+p_3P_2(\cos\ \theta),$$
$$B(\theta;p_4)=1+p_4P_1(\cos\ \theta). \tag{9}$$

The derivatives of the anisotropic part of the trial wave function required for the local energy evaluation were calculated numerically in the present work. In the course of a related study of heavier rare gas complexes[44] we recently derived compact and efficient analytical expressions for the local energy and the additional quantum drift force which appears in the diffusion quantum Monte Carlo algorithm [Eq. (13)] for the case of anisotropic trial wave functions.

For the larger clusters the VMC optimization did not lead to a statistically significant result for the anisotropic part of Ψ_T and consequently the following isotropic versions $\chi^{(2)}$ and $\chi^{(3)}$ were used

$$\chi^{(2)}(r;\vec{p})=\ \exp\left[-\frac{p_1}{r^5}-\frac{p_2}{r^2}\right]\cdot\frac{1}{1+\ \exp((r-p_3)p_4)},$$
$$\chi^{(3)}(r;\vec{p})=\ \exp\left(-\ \ln 2\left(\frac{p_1}{r}\right)^5-p_2r^{p_3}\right)\cdot r^{p_4}. \tag{10}$$

The shape of $\chi^{(2)}$ was inspired by the radial density of clusters with more than about 50 atoms, which exhibit a broad and rather flat density plateau beyond the first neighbor maximum (see Fig. 2). The Fermi function in the second part of $\chi^{(2)}$ describes an exponential edge of the wave function at large radii with a position controlled by p_3. Functions of this type have been successfully used before in the description of large helium clusters doped with xenon atoms.[45,46] Negative values for p_2 in $\chi^{(2)}$ can be used to describe a density maximum at short range. For clusters of intermediate size we carried out some calculations with $\chi^{(3)}$ which allows a more flexible description of the asymptotic shape of the wave function. Test calculations with a variant of $\chi^{(2)}$,

$$\chi^{(4)}(r;\vec{p})=\ \exp\left[-\ \ln 2\left(\frac{p_1}{r}\right)^5\right]\cdot\frac{1}{1+\ \exp((r-p_2)p_3)}$$
$$\times\exp(p_4\ \exp[-((r-p_5)p_6)^2]), \tag{11}$$

which includes an additional Gaussian lobe intended to describe the second nearest neighbor maximum in the pair correlation function, did not yield the expected improvements of the total energies.

B. Diffusion quantum Monte Carlo method

The diffusion quantum Monte Carlo (DMC) method[47] has been extensively discussed in a number of papers.[32–35,42] This section serves to summarize the main features of the method, our particular implementation, and some specific extensions developed for the present application.

The key idea of the DMC method is the isomorphism between the time dependent many body Schrödinger equation and a multidimensional reaction diffusion equation with anisotropic diffusion coefficients. Introduction of imaginary time $\tau=it/\hbar$, shifting of the absolute energy scale by a quantity $E_{\rm ref}$, and identification of the inverse mass terms with diffusion coefficients D_j and of the shifted potential $V(\vec{r})-E_{\rm ref}$ with position dependent rate terms $k(\vec{r})$ leads to the following equations which show this analogy:

$$i\hbar\frac{\partial\Psi(\vec{r},t)}{\partial t}=-\sum_j\frac{\hbar^2}{2m_j}\nabla_j^2\Psi(\vec{r},t)$$
$$+\{V(\vec{r})-E_{\rm ref}\}\Psi(\vec{r},t),$$
$$\frac{\partial\Psi(\vec{r},\tau)}{\partial\tau}=\sum_j\frac{\hbar^2}{2m_j}\nabla_j^2\Psi(\vec{r},\tau)-\{V(\vec{r})-E_{\rm ref}\}\Psi(\vec{r},\tau), \tag{12}$$
$$\frac{\partial C(\vec{r},t)}{\partial t}=\sum_j D_j\nabla_j^2C(\vec{r},t)-k(\vec{r})C(\vec{r},t).$$

Knowledge of the structure of the wave function can be fruitfully exploited for increased accuracy by introducing a guiding function Ψ_T approximating the true wave function. We used the isotropic part of our best VMC trial wave functions for this purpose. The introduction of Ψ_T results in additional drift terms in the diffusion equation which direct the random walkers into regions where the trial wave function is large. At the same time the rate terms are now controlled by the local energy [Eq. (4)] which is a much smoother function of the coordinates than the potential which reduces the variance of the energy estimators

$$\frac{\partial(\Psi\Psi_T)}{\partial\tau}=\sum_j\left\{\frac{1}{2m_j}\nabla_j^2(\Psi\Psi_T)-\frac{1}{m_j}\nabla_j(\Psi\Psi_T\nabla\ \ln\ \Psi_T)\right\}$$
$$-\{\Psi_T^{-1}\hat{T}\Psi_T+V(\vec{r})-E_{\rm ref}\}(\Psi\Psi_T). \tag{13}$$

This equation reduces to Eq. (12) for the trivial case of $\Psi_T=1$.

A random walk technique is used to calculate the steady state solution of the diffusion equation corresponding to a given quantum problem. A large ensemble of random walkers is propagated with time steps $\Delta\tau$ starting from some

arbitrary initial distribution. The propagation from τ to $\tau+\Delta\tau$ consists of random Gaussian displacements of the Cartesian coordinates and systematic moves under the influence of the quantum drift force $F(\vec{r})=\Psi_T\nabla \ln \Psi_T$ and an update of a weight carried by each random walker. Additionally we use a Metropolis type acceptance check for each attempted move[34] such that for arbitrary time steps the number density of walkers is given by Ψ_T^2 in the limit of zero branching, while their weights are a stochastic sample of the local value of Ψ/Ψ_T. This has been shown to result in large reductions of the time step error of DMC calculations.[35] Our implementation uses a global check after trial moves have been made for all particles. The short time approximation to the Green's function appropriate for Eq. (13) is

$$G(\vec{r}\rightarrow\vec{r}';\Delta\tau) = \prod_j \left[\left(\frac{m_j}{2\pi\Delta\tau} \right)^{3/2} \exp\left\{ -\frac{m_j}{2\Delta\tau}\left(\vec{r}_j-\vec{r}_j'-\frac{\Delta\tau}{2m_j}\vec{F}_j(\vec{r}) \right)^2 \right\} \right] \times \exp\left\{ -\Delta\tau_{\rm eff}\left(\frac{E_{\rm local}(\vec{r})+E_{\rm local}(\vec{r}')}{2}-E_{\rm ref} \right) \right\}. \quad (14)$$

The modified time step $\Delta\tau_{\rm eff}$ appears in the growth term of Eq. (14) because not all moves attempted according to $G(\vec{r}\rightarrow\vec{r}';\Delta\tau)$ are accepted in the Metropolis step. Proposed moves from $\vec{r}$ to $\vec{r}'$ are carried out with probability

$$P(\vec{r}\rightarrow\vec{r}')=\min\{1,A(\vec{r}\rightarrow\vec{r}')\},$$

$$A(\vec{r}\rightarrow\vec{r}')=\frac{|\Psi_T(\vec{r}')|^2 G(\vec{r}'\rightarrow\vec{r})}{|\Psi_T(\vec{r})|^2 G(\vec{r}\rightarrow\vec{r}')}. \quad (15)$$

The asymmetric transfer function $G(\vec{r}\rightarrow\vec{r}';\Delta\tau)$ has to be explicitly taken into account in this acceptance decision. The effective time step $\Delta\tau_{\rm eff}$ is defined through the ratio of accepted displacements and attempted displacements according to

$$\Delta\tau_{\rm eff}=\Delta\tau\frac{\langle\Delta\vec{r}^2\rangle_{\rm acc}}{\langle\Delta\vec{r}^2\rangle_{\rm att}}. \quad (16)$$

With the actual time steps used for our simulations the acceptance rates were between 99.9% for small clusters and 98% for the largest system with 200 particles.

The successive application of the components of the propagator $G(\vec{r}\rightarrow\vec{r}';\Delta\tau)$ causes a systematic error for finite $\Delta\tau$ which has to be eliminated by the use of sufficiently small time steps or calculations at several values of $\Delta\tau$ and extrapolation to $\Delta\tau=0$. The leading time step error is of order $\mathcal{O}(\Delta\tau^2)$ for the case $\Psi_T=1$ because of the neglect of commutators between $\hat{V}$ and $\hat{T}$. The customary simple integration scheme for the drift term caused by nontrivial trial wave functions leads to an additional time step error which is linear with $\Delta\tau$ but usually of much smaller absolute magnitude. The leading linear time step error is, however, observed only for very accurate trial wave functions.[35,44]

Our specific implementation assigns a variable weight to each random walker. As a consequence of the exponential weight update the sum of weights $W(\tau)=\Sigma_i w_i(\tau)$ grows or decays according to the mismatch between $E_{\rm ref}$ and the average local energy. Walkers whose relative weight $w_{\rm rel}=w_i/W(\tau)$ falls below a preselected value $w_{\rm min}$ are eliminated randomly from the ensemble with probability $p_-=1-w_{\rm rel}$ or retained and assigned the average weight $W(\tau)/n_{\rm walk}$ with probability $p_+=w_{\rm rel}$. Walkers whose relative weight grows beyond a maximum value $w_{\rm max}$ are split into $n_w=\text{int}(w_{\rm rel}+u)$ walkers of weight w_i/n_w, where u is a uniform random number. The values of $w_{\rm min}$ and $w_{\rm max}$ are chosen such that the average number of walkers remains approximately constant during the run, while the instantaneous ensemble size fluctuates. These mechanisms ensure that the walkers remain concentrated in relevant regions of configuration space without introducing artificial sources or sinks and can be easily generalized to a situation with correlated walks on several surfaces.[44,48]

After equilibration of the initial random walker distribution the ensemble average of $E_{\rm local}$ which will be referred to as $E_{\rm mean}$ in this paper is identical with the ground state energy irrespective of Ψ_T and is only subject to statistical fluctuations. The ground state energy can also be computed from the rate at which the total weight of the ensemble grows or decays as τ elapses. This estimator is called the growth energy

$$E_{\rm growth}=E_{\rm ref}-\frac{\partial \ln W(\tau)}{\partial\tau} \quad (17)$$

and is known to have a smaller time step dependence than $E_{\rm mean}$.[32] Both energy estimators were always extremely close to each other in our simulations, the difference never exceeding half the standard deviation of the energies. We therefore report only our values for $E_{\rm growth}$ as E_0 values.

The equilibrated distribution of weighted random walkers is given by $\Psi\Psi_T$ which can serve as an approximation to $|\Psi|^2$ for the calculation of expectation values if $\Psi_T\approx\Psi$ (see Sec. II C). Projections of the wave function on arbitrary coordinates can be obtained by binning the random walker coordinates into histograms. The construction of histograms turns out to be an efficient method for the construction of guiding functions.[44]

C. Calculation of expectation values

We calculate expectation values at various levels of accuracy. The simplest approximation is derived from the VMC calculation. Once an optimal wave function with parameters $p_{\rm opt}$ has been found, arbitrary property expectation values $\langle\hat{A}\rangle$ are computed by replacing integrals by sums over samples from the VMC distribution $|\Psi_T|^2$

$$\langle \hat{A} \rangle = \frac{\int \Psi_T^*(\vec{r};\vec{p}_{\rm opt}) \hat{A} \Psi_T(\vec{r};\vec{p}_{\rm opt}) d\vec{r}}{\int |\Psi_T(\vec{r};\vec{p}_{\rm opt})|^2 d\vec{r}}$$
$$\approx \frac{1}{N} \sum_{i=1}^{N} \Psi_T^{-1}(\vec{r}_i;\vec{p}_{\rm opt}) \hat{A} \Psi_T(\vec{r}_i;\vec{p}_{\rm opt}). \quad (18)$$

This scheme can be applied to local and nonlocal operators. Only expectation values of local operators are directly accessible with the DMC scheme. For both VMC and DMC algorithms the integration reduces to an average over operator values $A(\vec{r})$

$$\langle \hat{A} \rangle \approx \left(\sum_i^N w_i A(\vec{r}_i) \right) \Big/ \left(\sum_i^N w_i \right), \quad (19)$$

where w_i is 1 in the VMC case and either the current relative weight of the random walker or its weight multiplied by the sum of descendant weights,[49] respectively, in the DMC case. Usage of the random walkers' instantaneous weights amounts to a ''mixed'' expectation value $\langle \Psi | \hat{A} | \Psi_T \rangle$. We improve the correctness of mixed DMC expectation values by computing the extrapolated quantity

$$\langle \Psi | \hat{A} | \Psi \rangle = 2 \langle \Psi | \hat{A} | \Psi_T \rangle - \langle \Psi_T | \hat{A} | \Psi_T \rangle + \mathcal{O}(\Delta \Psi^2);$$
$$\Delta \Psi = \Psi - \Psi_T \quad (20)$$

and by additional collection of descendant weights to generate a statistical estimate of the true $|\Psi|^2$ distribution.[49] All histograms shown in the figures and the scalar expectation values have been computed with descendant weights.

This technique is in particular applicable to the positional correlation functions which are very useful in visualizing the structure of the clusters. The radial distribution of helium atoms relative to the center of mass of the whole cluster is computed as

$$P_{\rm rad}(r) = \frac{1}{n} \sum_i^n \left\langle \frac{\delta(r_i - r)}{r^2} \right\rangle_{\rm walk}. \quad (21)$$

In a similar way we compute the discrete version of the helium pair correlation function according to

$$P_{\rm pair}(r) = \frac{2}{n(n-1)} \sum_{i<j}^{n} \left\langle \frac{\delta(r_{ij} - r)}{r^2} \right\rangle_{\rm walk} \quad (22)$$

and the helium–HF pair correlation function. Both expressions are normalized such that

$$\int_0^\infty P_{\rm rad,pair}(r) r^2 dr = 1. \quad (23)$$

The radial distribution function can be easily converted to the spherically averaged radial helium density distribution $\rho(r)$ using

$$n = 4\pi \int_0^\infty \rho(r) r^2 dr,$$
$$\rho(r) = \frac{n}{4\pi} P_{\rm rad}(r). \quad (24)$$

In a similar way we compute two-dimensional histograms in cylinder coordinates to analyze the density distribution $\rho(r,z)$ of helium around the HF molecule. The HF bond is chosen as the z-axis and the perpendicular distance of helium atoms to this axis defines the polar radius r. The origin coincides with the center of mass of HF and hydrogen is on the positive z-axis. The density distribution is computed as

$$\rho(r,z) = \frac{n}{2\pi} \sum_i \left\langle \frac{\delta(r_i - r)}{r} \delta(z_i - z) \right\rangle_{\rm walk},$$
$$n = 2\pi \int_0^\infty \int_{-\infty}^{\infty} \rho(r,z) r dr dz. \quad (25)$$

This quantity is accumulated on a grid which is equidistant in z and r^2 which eliminates the need to take square roots during the data collection.

D. Adiabatic treatment of the HF vibration

The adiabatic separation introduces constraints into the dynamic treatment. Several schemes have been proposed for the modification of the DMC algorithm to properly account for these constraints.[36,50,51] Our scheme applies independent random displacements according to $G(\vec{r} \rightarrow \vec{r}\,';\Delta\tau)$ to both atoms of the diatomic subunit and modifies the resultant coordinates such that the center of mass of HF remains at the new position and contracts the HF bond vector to its prescribed length about the new center of mass. This guarantees the proper kinetic energy contribution of the center of mass of HF while correctly sampling the orientational space and the rotational kinetic energy. The fixed bond length used in this step is computed from the rotational constant for the relevant vibrational state as $r_{v;\rm rot} = \hbar/(2\mu B_v)^{1/2}$. It has to be distinguished from the HF bond length used in the evaluation of the adiabatic potential and discussed in Sec. II F.

The small violation of the constraint during the time step leads to a new time step error of order $\Delta\tau^2$, whose absolute size appears, however, not to be large. This is equivalent to the quadratic time step error of schemes which apply random rotations to the diatomic.[51] Our use of isotropic trial wave functions which act only on the center of mass of the diatomic guarantees that the drift step does not violate the constraint. Drift implementations with angle dependent forces or forces acting independently on the atoms of the fixed subunit require special care and may need higher order integration schemes over the time step to improve the simple straight line drift of Eq. (14).[44]

E. Frequency shift estimates

Since the energy difference $\Delta E_{\rm free}$ between a free HF molecule in its ground ($v=0$) and first excited vibrational state ($v=1$) at infinite separation from the helium cluster is known (3961.42 $\rm cm^{-1}$ [52]), the transition frequency of HF in the cluster can be related to this value by

$$\Delta E_{\rm matrix} = \Delta E_{\rm free} + E_{0;v=0} - E_{0;v=1}, \quad (26)$$

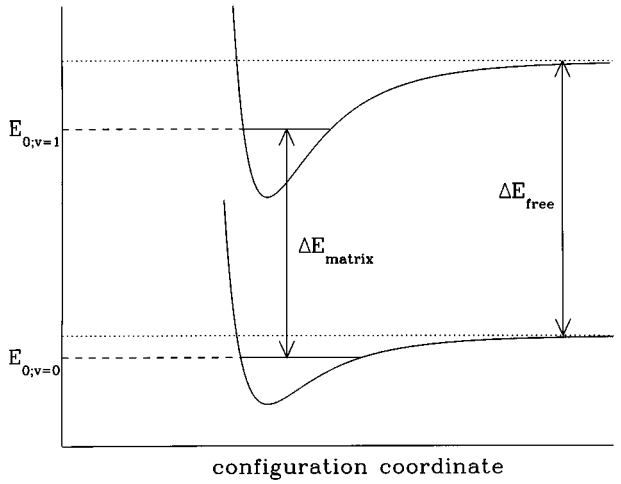

FIG. 3. Scheme for the calculation of adiabatic frequency shifts. The asymptote on the right represents separated helium atoms and free HF in the $v = 0$ (lower curve) and $v = 1$ (upper curve) vibrational state. The wells represent HF inside the helium cluster. The upper adiabatic well is deepened upon HF excitation and becomes narrower. The increased zero point energy partially compensates the deepening of the well. All effects are exaggerated in the graph.

where the energies $E_{0;v}$ are measured relative to the dissociation limit of completely separated helium atoms and free HF in the corresponding vibrational state (see Fig. 3) which defines the zero of the energy scale for each adiabatic surface. All $E_{0;v}$ values are consequently negative. The value for the frequency shift can accordingly be obtained from two separate calculations of the ground state energy on the adiabatic surfaces for $v=0$ and $v=1$, respectively, as

$$\Delta\nu=\Delta E_{\text{matrix}}-\Delta E_{\text{free}}=E_{0;v=0}-E_{0;v=1}. \tag{27}$$

Our first set of shift calculations was done in precisely this way. The main problem is the very small size of the shift relative to the absolute energies $E_{0;v}$ which requires very accurate ground state calculations. In the following discussion the symbol $E_{v=i}$ is used as an abbreviation for $E_{0,v=i}$.

Small energy differences are notoriously difficult to compute with Monte Carlo techniques. A very large computational effort has to be invested to achieve sufficiently small error bars for quantitative shift predictions. The problem is due to the superposition of individual errors in evaluations of two random quantities x and y according to

$$\begin{aligned}&\text{Var}\{x+y\}=\text{Var}\{x\}+\text{Var}\{y\}+2\,\text{Covar}\{x,y\},\\&\text{Var}\{x\}=\langle x^2\rangle-\langle x\rangle^2;\quad \text{Covar}\{x,y\}=\langle xy\rangle-\langle x\rangle\langle y\rangle,\end{aligned} \tag{28}$$

where the covariance is zero for uncorrelated samples. Deliberate introduction of correlations (large covariance) can be exploited to achieve greatly enhanced accuracy in a variety of applications.[31,40,53] A trivial case would be a relation like $x+y=\text{const}$ where the covariance exactly cancels the variances to give the expected zero variance for the constant sum. The reweighting technique applied in the VMC optimization is one application where one tries to exploit $x\approx y$ independent of fluctuations for x.

Correlations of this kind could in principle be exploited in our case of two adiabatic Hamiltonians $\hat{H}_{v=0}$ and $\hat{H}_{v=1}$

$$\begin{aligned}\hat{H}_{v=0}&=\hat{T}^{\text{He}}+\hat{T}^{\text{HF}}_{\text{com}}+\hat{T}^{\text{HF}}_{\text{rot};v=0}+\hat{V}_{v=0},\\\hat{H}_{v=1}&=\hat{T}^{\text{He}}+\hat{T}^{\text{HF}}_{\text{com}}+\hat{T}^{\text{HF}}_{\text{rot};v=1}+\hat{V}_{v=1},\\\hat{H}_{v=1}&=\hat{H}_{v=0}+\hat{T}^{\text{HF}}_{\text{rot};v=1}-\hat{T}^{\text{HF}}_{\text{rot};v=0}+\hat{V}_{v=1}-\hat{V}_{v=0},\\\hat{H}_{v=1}&=\hat{H}_{v=0}+\hat{T}^{\text{HF}}_{\text{rot};v=1}-\hat{T}^{\text{HF}}_{\text{rot};v=0}+\Delta\hat{V},\end{aligned} \tag{29}$$

where $\hat{T}^{\text{He}}$ is the kinetic energy operator for all helium atoms, $\hat{T}^{\text{HF}}_{\text{com}}$ is the kinetic energy associated with the center of mass motion of HF, and $\hat{T}^{\text{HF}}_{\text{rot};v}$ is the kinetic energy operator associated with rotational motion of HF. The latter part is a parametric function of v because of the dependence of the HF moment of inertia on its vibrational excitation. The two Hamiltonians differ only in the kinetic energy term describing the rotation of the rigid diatomic and the small change in the shape of the adiabatic HF–He potential $\Delta\hat{V}$. Provided the same trial wave function is used in the DMC calculation, the potential difference only affects the growth rate and thereby the weights of the random walkers. The presence of different potentials presents no problems for a scheme where the same set of random walks is executed synchronously on two (or more) surfaces.[36,44] The existence of common terms in the potentials can also lead to great computational savings.

The excitation dependent constraint on the HF bond length does however force different configurations to be visited and prevents the direct application of the correlation technique without further modifications. For this type of problem we have, however, developed modifications of the correlation technique which we will describe in detail in a forthcoming paper.[48]

Another way of reducing the variance of the shift estimate is a perturbational treatment of the potential difference $\Delta V(\vec{r})$. Assuming that the wave functions on both adiabatic surfaces are similar, $\Psi_{v=1}=\Psi_{v=0}+\Delta\Psi$, we can write

$$\begin{aligned}\langle E_{v=1}\rangle&=\langle\Psi_{v=1}|\hat{H}_{v=1}|\Psi_{v=1}\rangle\\&=\langle\Psi_{v=0}+\Delta\Psi|\hat{T}_{v=1}|\Psi_{v=0}+\Delta\Psi\rangle\\&\quad+\langle\Psi_{v=0}+\Delta\Psi|\hat{V}_{v=0}+\Delta\hat{V}|\Psi_{v=0}+\Delta\Psi\rangle\\&=\langle E_{v=0}\rangle+\underbrace{\langle\Psi_{v=0}|\Delta\hat{V}|\Psi_{v=0}\rangle}_{\Delta\nu}+\mathcal{O}(\Delta\Psi).\end{aligned} \tag{30}$$

In the last step we also used the approximation $\hat{T}_{v=1}\approx\hat{T}_{v=0}$ or rather that the expectation value of $\Delta\hat{T}_v$ is very small. This term is exactly zero in the free rotor limit. Our numerical tests showed that $\langle\Delta\hat{T}_v\rangle$ is indeed statistically indistinguishable from zero for HF in helium clusters. The expectation value of the adiabatic potential difference is computed during a ground state simulation with the techniques described in Sec. II C. The advantage of this approximate scheme is a sharp reduction of statistical fluctuations because of the near constant behavior of $\Delta\hat{V}$. The statistical error for $\langle\Delta V\rangle_0=\langle\Psi_{v=0}|\Delta\hat{V}|\Psi_{v=0}\rangle$ is about an order of magnitude smaller than the error bars for the total energies.

In order to obtain an estimate of the systematic error, we applied the same scheme in the opposite direction by averaging $\Delta\hat{V}$ over the upper adiabatic wave function in simulations on the adiabatic surface with vibrationally excited HF (see Sec. II F). This yields the estimate $\langle \Delta V \rangle_1$. The two estimates of the perturbational frequency shift agreed with each other typically within 5% (see Table II). Agreement is also very good with first results from direct correlated estimates of the frequency shift which does not involve any approximation.[48]

F. Potential energy surface

All calculations were done with a purely pairwise additive potential energy surface based on an *ab initio* part for the HeHF interaction[25] and the empirical HFD-B potential for He.[26] The original HeHF surface is an explicit function of three Jacobi coordinates. Our initial plan to compute the ground state energy of the cluster with freely vibrating HF failed because the HeHF part of the surface has some unphysical features at large HF bond extensions which are sampled with nonvanishing probability. These features result from the fitting procedure adopted for the construction of an analytical representation of the original *ab initio* potential values. A readjustment of the analytical representation[25] for the largest HF distance used in the *ab initio* calculations ($1.918\ a_0$) improved the smoothness of the surface but could not completely remove the problem. As a consequence of this readjustment the surface in the present treatment differs slightly from the originally published version.

For the adiabatic calculations we replaced the full three-dimensional HeHF potential by the function

$$V_v^{\mathrm{HeHF}}(r,\theta) = V^{\mathrm{HeHF}}(r,\theta,r_v) \tag{31}$$

where $r_v = \langle r_{\mathrm{HF}} \rangle_v$ is the expectation value of the HF distance in the vibrational state with quantum number v. This is a further approximation beyond the usual adiabatic expression

$$V_v^{\mathrm{HeHF}}(r,\theta) = \langle V^{\mathrm{HeHF}}(r,\theta,r_{\mathrm{HF}}) \rangle_v , \tag{32}$$

where the index v indicates averaging over the HF wave function. This operation could not be carried out in a reliable way because of the aforementioned problems at large r_{HF}. However, Eq. (31) is a good approximation because of the relative compactness and near symmetry of the HF vibrational ground state wave function. The HF wave functions used for the determination of r_v were computed numerically[54] from Huffaker's HF potential function.[55] For the two relevant vibrational states of HF the expectation values r_v lie well within the range where the *ab initio* surface is free from unphysical behavior. The actual r_v values and the B_v values used to calculate the fixed bond length constraint $r_{v;\mathrm{rot}}$ (see Sec. II D) in our calculations are collected in Table I.

Within this approximation the adiabatic potential of the He_nHF cluster is now expressed as

$$V_{\mathrm{total}} = \sum_{i=1}^{n} V_v^{\mathrm{HeHF}}(r_i,\theta_i) + \sum_{i<j}^{n} V^{\mathrm{HeHe}}(r_{ij}), \tag{33}$$

TABLE I. Molecular data for HF used in the adiabatic calculations for He_nHF clusters.

v	r_v/Å [a]	B_v /cm^{-1} [a,b]	$r_{v;\mathrm{rot}}$/Å [a]	r_v/Å[c]	B_v /cm^{-1} [c]
0	0.9329	20.559743	0.9256	0.9257	20.5555
1	0.9652	19.787478	0.9434	0.9436	19.7834

[a]Values used in our calculation.
[b]Taken from Ref. 39
[c]Values used in Ref. 29; no distinction was made between $r_{v;\mathrm{rot}}$ and r_v.

with coordinate definitions as in Eq. (7). The HeHF surface has been completely reprogrammed to allow full pipelining and parallel execution. The new implementation has been extensively checked against the original source code kindly provided by Moszynski[25] by evaluations at several million randomly distributed geometries and no deviations exceeding a few times the machine roundoff were found.

The adiabatic HeHF surfaces for $v=0$ and $v=1$ are displayed in Fig. 1. Two almost equivalent wells at linear geometries are separated by a barrier in the T-shaped geometry. The wells at $\theta=0$ (helium on the hydrogen side) and $\theta=\pi$ have depths of -36.9 cm^{-1} and -40.1 cm^{-1}, respectively, for $v=0$. The barrier is at about -18.8 cm^{-1} and $\theta=\pi/2$. The equilibrium Jacobi distances for the minima are about 6.1 a_0 for $\theta=0$ and 5.35 a_0 for $\theta=\pi$. The well at $\theta=\pi$ actually becomes progressively deeper than the $\theta=0$ well with vibrational excitation of HF (extension of the HF bond) while the $\theta=0$ well is rather insensitive. This apparent strong anisotropy is, however, removed almost completely by quantum mechanical delocalization since already the ground state energy of HeHF of -7.50 cm^{-1} by far exceeds the barrier and leads to an almost isotropic helium density distribution around HF (see Figs. 4 and 7). This strong delocalization also compensates the deepening of the well at $\theta=\pi$ upon HF excitation, which would lead to a classical He$\cdots$FH structure and leads to a small maximum at $\theta=0$ in the quantum mechanical probability distribution shown in Fig. 4.

G. Computational details

The cost for the He–He part of the potential surface and the trial wave function and local energy grows quadratically with the number of helium atoms due to the pairwise additive and multiplicative model, respectively. Since the evaluation of the HeHF interactions is much more costly, this part dominates the effort such that in practice the computational cost for the treatment of He_nHF scales only linearly with n up to about $n=100$.

The VMC runs consisted of between 4×10^5 and 10^6 steps with uniformly distributed step sizes adjusted to yield an acceptance rate close to 0.5 (typically about 2 a_0). Atoms were moved one by one and energy samples were taken after typically 5 moves. The serial correlation was analyzed by computation of the energy autocorrelation function and taken into account in the variance estimation.

All DMC calculations were done with an ensemble of variable size kept at an average size of 1000 random walkers

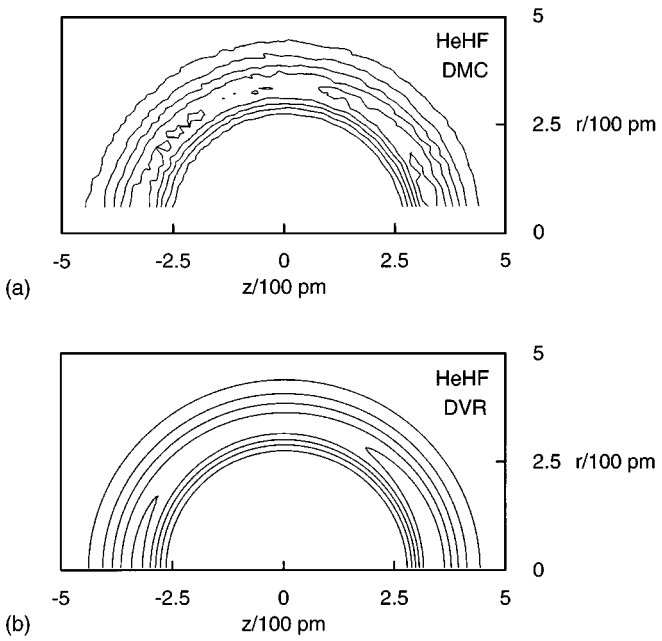

FIG. 4. Two-dimensional helium density in cylinder coordinates z and r [Eq. (25)] for HeHF from DMC (top) and DVR-DGB calculations (bottom). Contour levels are at 0.001, 0.002, 0.003, 0.004, 0.005, and 0.006 Å^{-3}.

by proper choice of $w_{\min}$ and $w_{\max}$ and ensemble renormalization at the end of each block of steps. The good quality of our trial wave functions allowed the use of time steps of $\Delta\tau = 200$ a.u. without any noticeable time step bias. The computation of energy differences is even more robust with respect to the time step because of error cancellation. The effective time steps were very close to the nominal time step with $\Delta\tau_{\text{eff}}$ never smaller than $0.98\ \Delta\tau$.

Initial ensembles from VMC calculations were propagated for several thousand steps for equilibration. Energy estimators were collected over blocks with sufficient length for correlations to die out (50–200 steps depending on cluster size) and to allow the collection of converged descendant weights. Serial correlations between block averages were quantified through the calculation of autocorrelation functions. The correlation corrected error estimates thus obtained from single runs were always consistent with estimates obtained from groups of completely independent runs. The number of blocks over which averages were taken was varied according to cluster size to obtain the desired accuracy. A typical value is 100 blocks. All quoted errors are one standard deviation.

To guard against subtle systematic errors introduced by the pseudo random number generator[56,57] we made test runs with different combinations of uniform generator and method for the transformation into Gaussian deviates. Since we did not detect any problems we used the fastest combination, namely a vectorized floating point subtractive implementation of the R250 generator[58] in combination with Box–Muller transformation.[59]

Our DMC program is fully vectorizable and very well suited to parallel computers. Initial runs and production runs for small clusters were done on RS6000, DEC AXP3800 workstations, and a DEC AlphaServer 2100 5/250. DMC production runs for large clusters were done on a 4 processor SGI Power Challenge on which a parallel efficiency very close to one was achieved. The largest calculation with 200 particles consumed about 100 hours on the Power Challenge.

III. EXPERIMENT

The experiments have been carried out in a molecular beam apparatus which has been described earlier.[60,61] A detailed description of the current experimental setup may be found in a very recent publication devoted to the vibrational spectroscopy of water molecules and small water polymers embedded in large liquid helium clusters.[62] Therefore, a brief description concentrating on the important aspects is sufficient.

The helium clusters (He_n) were produced by adiabatic expansion of helium gas through a 5-μm-diameter nozzle kept at a temperature of $T_0 = 21.0$ K. The stagnation pressure was $p_0 = 40$ bar. Under these conditions we obtained a log-normal helium cluster size distribution with a mean cluster size of $\langle n \rangle = 2000$. The helium cluster beam was characterized in a separate experiment,[63] employing the procedure described in Ref. 7.

After having passed the 15 cm long pick-up chamber, which was filled with HF molecules at a partial pressure of $p_{\text{HF}} = 2\times10^{-5}$ mbar, and three differential pumping stages, the helium clusters entered the innermost detector chamber containing the electron bombardment ionizer (electron energy = 100 eV), quadrupole mass spectrometer (mass range = 0–150 amu), and ion multiplier. Due to the collisions with the chromophore molecules in the pick-up chamber, approximately 20% of the helium clusters were doped with HF molecules. The pick-up pressure of $p_{\text{HF}} = 2\times10^{-5}$ mbar was sufficiently low to keep the concentration of HF dimers embedded in helium clusters at a negligible level. As a result of the embedding of a HF molecule into the helium cluster, approximately 600 helium atoms are evaporated. This value has been estimated following the results of Lewerenz *et al.*[8] who found that 635 helium atoms were evaporated when a H_2O molecule was embedded under similar conditions. Thus, after embedding of the HF molecule, the composite He_nHF cluster should contain approximately 1400 helium atoms.

Before entering the detector chamber through a pinhole of 0.2 mm diameter, the pure and chromophore-containing helium clusters were subjected to an intense infrared (IR) laser beam in the quasicoaxial configuration in which the counterpropagating laser intersected the cluster beam at a small angle.[60] The tunable infrared radiation was obtained from a recently developed injection-seeded optical parametric oscillator (OPO).[64] It consisted of a master oscillator containing a 5-cm-long $LiNbO_3$ crystal and a difference frequency mixing stage with a 25-mm-long $LiIO_3$ crystal in which the 2.5 μm-radiation used for seeding the master oscillator was generated. The typical output energy was 4 mJ/pulse with a bandwidth of 0.25 cm^{-1}, the latter being deter-

mined by the spectral width of the dye laser. Wavelength calibration was performed by measuring the absorption spectrum of HF in a photoacoustic cell and comparing the experimental line positions with those of the HITRAN92 data base.[65]

When the HF molecules embedded in the helium clusters are vibrationally excited the vibrational energy is transferred to the helium host cluster on a very short time scale. In turn, the excess energy is rapidly released by evaporating a few hundred He atoms. Assuming a helium binding energy of 7.2 K,[66] the absorption of a 4000 cm^{-1}-photon results in the evaporation of approximately 700 He atoms. As a consequence, the size of the chromophore-containing helium cluster is somewhat reduced leading to an effective reduction of its ionization cross section. Hence, it follows that the pulsed excitation of the HF molecule (in the helium cluster) can be detected by the transient decrease (depletion) of the signal monitored by the mass spectrometer on a characteristic mass. If the relative depletion is recorded as a function of laser frequency an absorption spectrum of HF embedded in helium clusters is obtained.

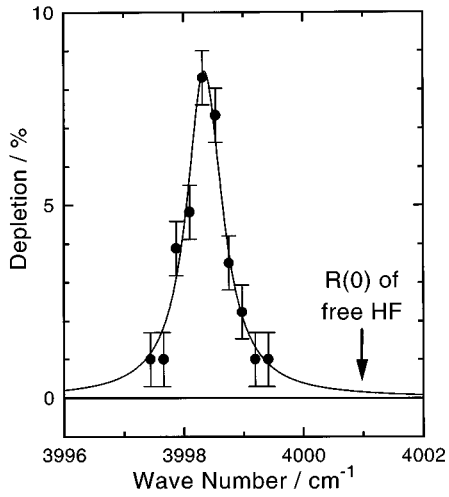

FIG. 5. The $R(0)$ line of HF embedded in He_n ($\langle n\rangle = 1400$) measured as a depletion spectrum on $m = 5$ amu (HeH^+). The other experimental conditions were as follows: $p_0 = 40$ bar, $T_0 = 21.0$ K (yielding an average helium cluster size (Ref. 63) of $\langle n\rangle = 2000$ prior to the deposition of the HF molecule), and $p_{HF} = 2\times10^{-5}$ mbar. The laser bandwidth was 0.25 cm^{-1}.

IV. RESULTS AND DISCUSSION

A. Experimental results

Employing various temperatures T_0 of the helium cluster source (i.e., helium cluster sizes) and HF pressures in the pick-up chamber, we have studied the effect of the deposition of HF molecules on the mass spectra. If, for a fixed helium cluster size, the density of HF molecules was gradually increased we observed at first the appearance of signal on the masses $m = 4k + 1$amu which can be readily assigned to the ionic complexes He_kH^+ ($k = 1,2,3,\ldots$). The largest signal was found for $k = 1$. Apparently these complexes are formed in an intracluster reaction following the ionization induced by electron impact according to

$$He_nHF \xrightarrow{e^-} He_nHF^+ \rightarrow He_kH^+ + F + (n-k)He. \quad (34)$$

Unfortunately the HF^+ ion has the same mass ($m = 20$ amu) as the helium cluster ion He_5^+. Due to this coincidence it was not possible to observe an increase on the corresponding mass peak which was dominated by He_5^+. When the HF pressure in the pick-up chamber was raised further, the formation of HF complexes was made possible as evidenced by the observation of significant signal on the masses $m = 20k + 1$ with $k = 1-7$. These mass peaks are assigned to $(HF)_kH^+$ ions produced during the ionization of $(HF)_n$ ($n \geqslant k + 1$) complexes embedded in large helium clusters.

In order to study the spectroscopy of HF molecules in helium clusters, the pick-up pressure should be kept as low as possible to avoid the formation of HF complexes in the helium cluster which might absorb in the same spectral region. Under the conditions employed for this experiment ($T_0 = 21.0$ K; $p_{HF} = 2\times10^{-5}$ mbar), the signal on $m = 21$ amu (HFH^+) was very small, indicating that HF dimers do not play a significant role. On the other hand, the height of the peak at $m = 20$ amu was practically not affected by the deposition of HF molecules. The only clear indication that HF molecules were embedded into the helium clusters was the observation of a strong signal on $m = 5$ amu (HeH^+) in the range of 10^4 counts s^{-1}. Thus, this mass seemed to be most suitable to study the absorption of HF in He_n.

Figure 5 shows the depletion spectrum we have measured with the mass spectrometer tuned to $m = 5$ amu. The other experimental conditions were mentioned and are resumed in the figure caption. The solid line represents a Lorentzian line shape function fitted to the experimental data. Its position and width have been determined to be $\tilde{\nu}_0 = 3998.35$ cm^{-1} and $\Gamma = 0.7$ cm^{-1} (full width at half-maximum), respectively. Due to the position of this absorption line, there is no doubt that it must be assigned to the $R(0)$ transition in the helium-embedded HF molecule. It is thus redshifted by 2.64 cm^{-1} from the $R(0)$ line observed for free gas phase HF molecules at 4000.989 cm^{-1}.[52]

As mentioned before, the laser system has been calibrated by measuring the absorption spectrum of gas phase HF in a photoacoustic cell. Noting that the frequency shift is rather small, we estimate the accuracy of the calibration in this frequency range to be better than 0.1 cm^{-1}. Together with the uncertainty of the fitted line position which is estimated to be 0.05 cm^{-1} we obtain for the overall error 0.15 cm^{-1}. Thus, the result of the present experiment is that the $R(0)$ line of HF embedded in a helium cluster containing approximately 1400 atoms (He_{1400}) is redshifted by 2.65 ± 0.15 cm^{-1}.

The linewidth of the absorption profile which has been determined by the fit to be 0.7 cm^{-1} is considerably broader than the laser bandwidth of 0.25 cm^{-1}. Assuming a Gaussian laser profile, we estimate that the linewidth of the transition is approximately 0.65 cm^{-1}. If this broadened linewidth is completely assigned to lifetime broadening we obtain the result that the vibrationally excited HF molecule in the $J = 1$ state has a lifetime of 8 ps, i.e., the corresponding vibra-

TABLE II. Total energies for He_nHF with HF, $v=0$ (E_0) and $v=1$ (E_1) and adiabatic frequency shifts from DMC and VMC calculations. ΔE is the energy difference estimate and $\langle \Delta V \rangle$ are perturbational estimates as explained in Sec. II E. All energies are given in cm^{-1}. The numbers in parentheses indicate the statistical error in units of the last digit.

n	E_0^{DMC}	E_1^{DMC}	ΔE	$\langle \Delta V \rangle_0^{\mathrm{DMC}}$	$\langle \Delta V \rangle_1^{\mathrm{DMC}}$	E_0^{VMC}	$\langle \Delta V \rangle_0^{\mathrm{VMC}}$
1	−7.503(7)	−7.70(1)	−0.19(1)	−0.190(3)	−0.202(2)	−7.154(6)[a]	−0.125[a]
2	−15.31(2)	−15.67(2)	−0.36(3)	−0.363(4)		−14.70(1)[a]	−0.38[a]
3	−23.36(3)	−23.93(3)	−0.57(4)	−0.533(5)		−22.70(1)[a]	−0.51[a]
4	−31.60(4)	−32.38(4)	−0.78(6)	−0.712(9)		−30.86(1)[a]	−0.67[a]
5	−39.9(1)	−40.9(1)	−1.0(1)	−0.88(1)	−0.94(1)	−38.77(1)[a]	−0.81[a]
6	−48.3(1)	−49.3(1)	−1.0(2)	−1.08(1)		−46.74(1)[a]	−0.98[a]
7	−56.6(1)	−57.8(1)	−1.2(2)	−1.25(1)		−54.19(2)[a]	−1.14[a]
8	−63.9(2)	−65.7(1)	−1.8(2)	−1.43(1)		−60.98(2)[a]	−1.28[a]
9	−71.3(2)	−73.2(1)	−1.9(2)	−1.62(2)		−66.75(2)[a]	−1.44[a]
10	−77.7(2)	−79.5(2)	−1.9(3)	−1.78(2)	−1.87(2)	−71.69(4)[a]	−1.56[a]
11	−82.5(2)	−84.6(2)	−2.1(3)	−1.93(2)		−74.52(4)[a]	−1.40[a]
12	−86.9(2)	−89.2(2)	−2.3(3)	−2.04(2)		−76.71(4)[a]	−1.55[a]
13	−90.4(2)	−92.5(2)	−2.1(3)	−2.10(2)		−78.87(5)[b]	−1.80[b]
14	−93.6(2)	−96.1(2)	−2.5(3)	−2.16(2)		−81.39(5)[b]	−1.84[b]
15	−96.3(2)	−98.9(2)	−2.5(3)	−2.18(2)	−2.27(3)	−82.39(5)[b]	−1.92[b]
16	−99.9(2)	−102.5(2)	−2.6(3)	−2.22(3)		−84.70(5)[b]	−1.83[b]
17	−102.5(2)	−105.0(2)	−2.5(3)	−2.26(3)		−86.81(5)[b]	−1.83[b]
18	−105.4(2)	−107.8(2)	−2.4(3)	−2.29(3)		−88.47(5)[b]	−1.75[b]
19	−108.0(2)	−110.7(2)	−2.7(3)	−2.32(3)		−91.03(5)[b]	−1.77[b]
20	−110.6(2)	−113.3(3)	−2.6(4)	−2.32(3)	−2.42(3)	−92.94(5)[b]	−1.89[b]
25	−124.4(3)	−126.7(3)	−2.2(5)	−2.45(3)	−2.52(3)	−102.78(7)[b]	−1.87[b]
30	−138.6(4)	−141.1(3)	−2.5(6)	−2.55(3)	−2.60(3)	−112.73(9)[b]	−1.89[b]
35	−155.2(6)	−157.4(6)	−2.2(9)	−2.59(4)	−2.72(4)	−123.6(1)[b]	−1.97[b]
40	−169.1(7)	−171.4(7)	−2.3(10)	−2.71(4)	−2.80(4)	−129.2(2)[b]	−1.82[b]
45	−179.1(6)	−182.1(6)	−2.9(9)	−2.79(4)	−2.88(4)	−138.0(2)[b]	−1.80[b]
50	−200.3(9)	−202.9(9)	−2.6(14)	−2.78(5)	−2.89(5)	−143.2(2)[b]	−1.94[b]
98	−347.0(1)	−349.8(1)	−2.8(1)	−2.70(5)	−2.85(8)		
100						−262(2)[c]	
198	−690.0(9)	−692.3(9)	−2.3(14)	−2.60(9)			
200						−561(1)[d]	

[a]Calculated with $\chi^{(1)}$ and the parameters given in Table III.
[b]Calculated with $\chi^{(3)}$ and the parameters given in Table IV.
[c]$\chi^{(2)}$ with $p_0=5.25\ a_0$, $p_1=4400\ a_0^5$, $p_2=-21.4\ a_0^2$, $p_3=17\ a_0$, and $p_4=0.37\ a_0^{-1}$.
[d]$\chi^{(2)}$ with $p_0=5.25\ a_0$, $p_1=4400\ a_0^5$, $p_2=-21.4\ a_0^2$, $p_3=19\ a_0$, and $p_4=0.37\ a_0^{-1}$.

tional energy is transferred to the phonon bath of the helium cluster within 8 ps. This energy is then dissipated by evaporating approximately 700 helium atoms. In this consideration we neglected the possibility that the absorption line could be affected by power broadening. Unfortunately it was not possible to measure a power dependence, in order to be able to account for this effect. But it should be noted that, if part of the broadening were due to power broadening, the actual lifetime would be longer.

B. Ground state energies and wave functions

The calculated adiabatic ground state energies for He_nHF in the HF vibrational states $v=0$ and $v=1$ from both VMC and DMC calculations for clusters of different sizes are collected in Table II. For the smallest system (HeHF) calculations with conventional quantum methods are also possible. In order to convince ourselves of the accuracy of our approach we made careful comparisons between QMC results and variational results for this system.

Due to the slightly modified analytical representation of the HeHF surface and our use of different r_v values in the adiabatic approximation our ground state energy of $-7.503 \pm 0.007\ cm^{-1}$ for HeHF cannot be directly compared with the original value of $-7.380\ cm^{-1}$ obtained by Moszynski *et al.*,[29] who also used r_v values calculated from B_v according to $r_v=\hbar/(2\mu B_v)^{1/2}$ (see Table I). These r_v values are smaller than ours and lead to an estimated upward shift of the ground state energy by approximately $0.044\ cm^{-1}$. The additional effect of the slightly modified surface is difficult to estimate but should be quite small. Since this clearly does not account for the observed discrepancy, we performed a set of DVR-DGB calculations[67] for HeHF with the HF parameters from Ref. 29 together with the original surface and with our set of $r_v, B_v, r_{\mathrm{rot}}$ values combined with the refitted surface. For the refitted surface the DVR-DGB runs initially seemed to converge to a ground state energy of $-7.45\ cm^{-1}$ which is more than seven σ higher than the DMC value. Using the same basis set in combination with the parameters from Moszynski *et al.* we obtained $-7.382\ cm^{-1}$ in very good agreement with the original result.[29]

Careful inspection of the DVR-DGB calculations, however, revealed sensitivities to the choice of basis parameters hinting at subtle problems in the description of the very diffuse radial part of the wave function by the distributed

TABLE III. Wave function parameters and VMC energies for small He_nHF clusters with HF in the $v = 0$ vibrational state calculated with wave function $\chi^{(1)}$ defined in Eq. (8). Numbers in parentheses indicate uncertainties in units of the last digit.

n	p_0/a_0	p_1/a_0	p_2/a_0^{-1}	p_3	p_4	E_0/cm^{-1}
1	⋯	6.502	0.5872	0.02202	−0.01562	−7.154(6)
2	6.096	6.902	0.8205	0.01540	−0.00156	−14.70(1)
3	5.605	6.802	0.8135	0.02766	−0.00601	−22.70(1)
4	5.399	6.797	0.8491	0.02009	0.01986	−30.86(1)
5	5.380	6.800	0.8800	0.03000	−0.00200	−38.77(1)
6	5.380	6.775	0.8820	0.03000	−0.00200	−46.74(1)
7	5.390	6.775	0.9025	0.00000	0.00000	−54.19(2)
8	5.400	6.730	0.9030	0.00000	0.00000	−60.98(2)
9	5.420	6.730	0.9030	0.00000	0.00000	−66.75(2)
10	5.400	6.750	1.0000	0.00000	0.00000	−71.69(4)
11	5.400	6.600	0.9000	0.00000	0.00000	−74.52(4)
12	5.400	6.600	0.8500	0.00000	0.00000	−76.71(4)

Gaussian basis. A modified code[68] which selectively improves the basis by using broader Gaussians at large Jacobi distances finally gave a ground state energy of -7.5036 cm^{-1} for HeHF with HF in the $v = 0$ vibrational state. Using this improved radial basis with the original surface and HF parameters gave an energy of -7.4167 cm^{-1}, significantly below the reported result of -7.380 cm^{-1}.[29] It appears that the radial Laguerre function basis used in the TRIATOM program suite[69] used by Moszynski *et al.* suffers from the same problems which we encountered with distributed Gaussians. We found a visible difference between the wave function giving $E_0 = -7.45$ cm^{-1} and the final one with $E_0 = -7.5036$ cm^{-1} in the peak amplitude and in particular in the long range tail. The latter was too compact and exhibited very small wiggles in the case of the higher energy wave function.

This problem, which is significant already in the ground state of the extremely floppy HeHF system, might occur also in highly excited vibrational states close to the dissociation limit in more strongly bound systems since it seems to be related to the diffuse nature of the radial component of the wave function. It might be related to the asymptotically incorrect form of Gaussians and other nonexponential basis functions, which can also cause problems in electronic structure calculations of properties other than the energy, which depend on the correct description of the long range behavior of the wave function.

The almost perfect agreement between the final DVR-DGB calculation and the DMC calculation on the modified surface gives us high confidence into our results for larger clusters and shows the power of the DMC method to describe ''exotic'' wave functions which turn out to be very resistant to traditional approaches. To our knowledge it is the first example of a subtle defect in a variational vibrational calculation being identified through an accurate quantum simulation.

The VMC wave function for HeHF with only four adjustable parameters (see Table III) gives a comparatively good representation of this very floppy system and recovers 95% of the binding energy ($E_{\mathrm{VMC}} = -7.154$ cm^{-1}). Generally the VMC energies for He_nHF are rather accurate upper bounds for the exact DMC values up to $n \approx 10$. For larger clusters the difficulty in constructing trial wave functions which correctly describe the density build up beyond nearest neighbors and the long range oscillations is reflected in the progressively worse VMC energies.

The total DMC energy of the He_nHF clusters plotted vs cluster size in Fig. 6 is an almost perfectly linear function of n up to $n \approx 10$ with a slope of about 11 K per helium atom. It should be noted that for most cluster sizes the error bars are much smaller than the size of the symbols in the graph. Similar additive behavior of the total energy has been observed previously in the related Cl_2He_n, $n = 1,\ldots,4$ systems[17] and could be rationalized in the framework of an additive zero point energy model. For clusters with more than 15 helium atoms the total energy has again a close to linear size dependence with a slope of about 5.5 K per helium atom. These

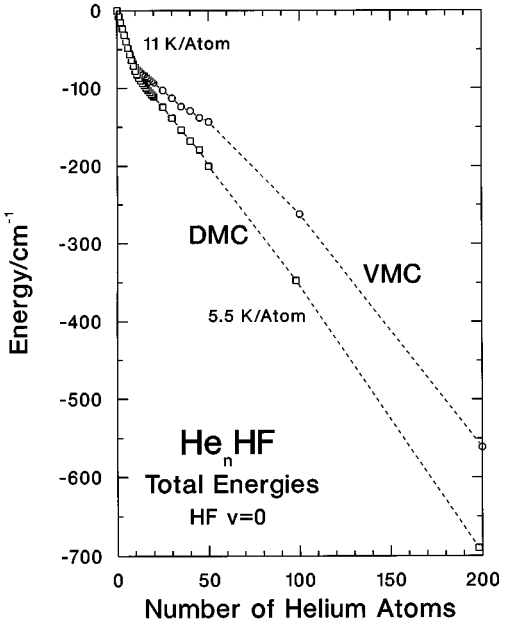

FIG. 6. Total energy of He_nHF vs cluster size from VMC (circles) and DMC (squares) calculations for HF in its vibrational ground state. Note the smooth size dependence and the inflection between 10 and 15 helium atoms.

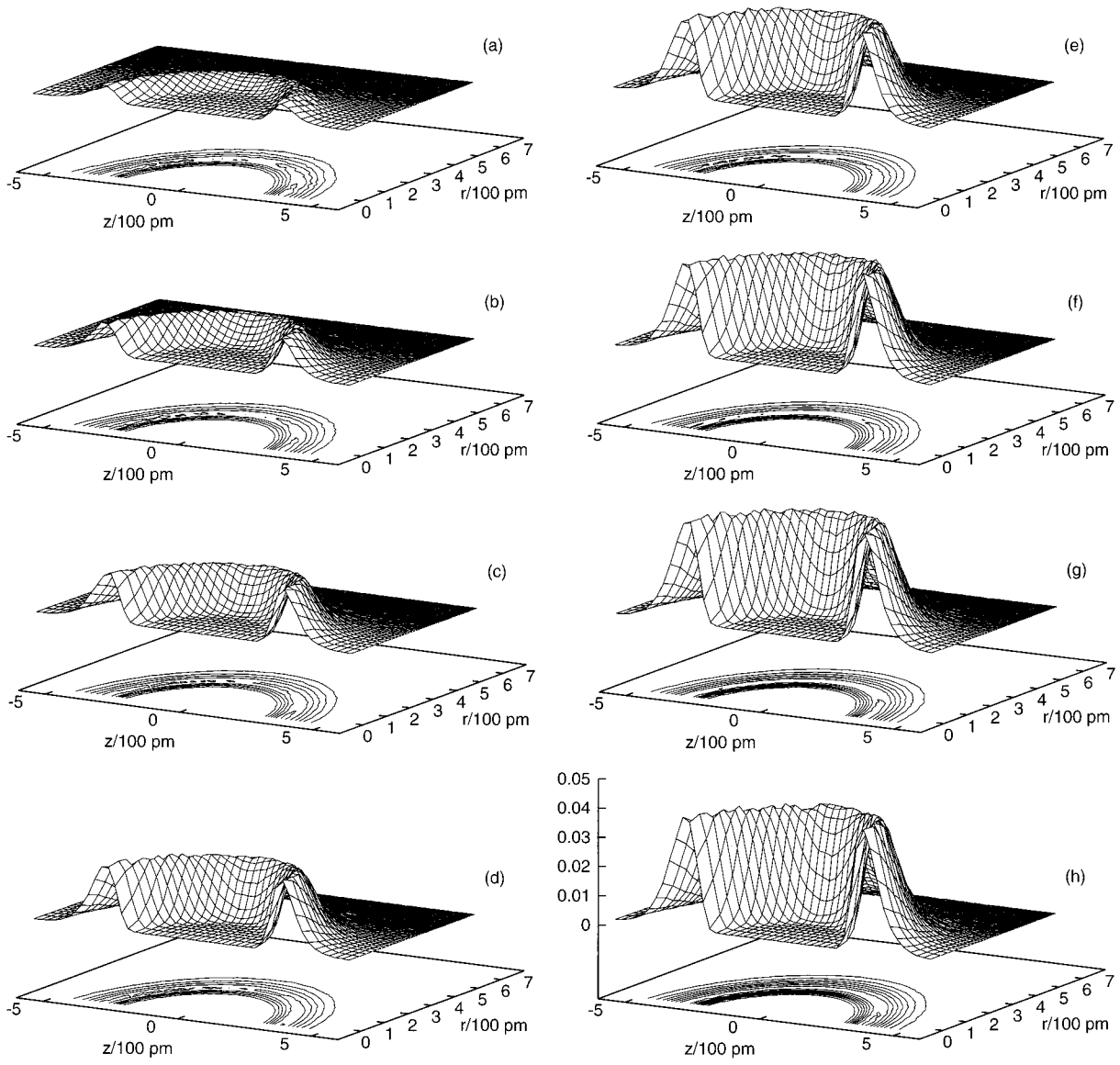

FIG. 7. Two-dimensional helium density in units of $Å^{-3}$ for several cluster sizes: (a) HeHF, (b) He_2HF, (c) He_3HF, (d) He_4HF, (e) He_5HF, (f) He_6HF, (g) He_7HF, (h) He_8HF. Note the linear density increase with cluster size without shape change and the nearly perfect isotropy of the distributions.

values have to be compared to the bulk helium binding energy of 7.2 K per particle.[66] The initial stronger binding energy is obviously due to the HF impurity, while the binding energy slowly approaches the bulk limit from below for larger clusters in agreement with results for pure helium clusters.[1,3,70,71] Close inspection does indeed reveal a weak trend towards a higher energy per particle for the largest clusters investigated.

Already the ground state energy of HeHF (-7.50 cm^{-1}) by far exceeds the height of the barrier located at about -18 cm^{-1} which separates the two linear minimum energy configurations (see Fig. 1). While this finding by itself is not unambiguous evidence for delocalization over both wells since the height of the adiabatic barrier is the relevant quantity, inspection of the HeHF wave function shows an extreme amount of delocalization where all orientations of HF relative to the helium atom have an approximately equal probability. The wave function corresponds to an almost free rotor as can be seen in Fig. 4 which shows the DMC result together with the variational wave function. This is in contrast to Ar_nHF clusters for which a strongly hindered HF rotor was found.[36,38,39,43,44]

Whereas Ar_nHF and Ar_nHCl clusters exhibit distinct isomerism there is no trace of isomerism in the He_nHF series because of the very high zero point energy. The known full delocalization of helium in pure helium clusters is not significantly reduced by the molecular impurity. This becomes clear on inspection of the density distribution of helium around HF shown in Fig. 7 for several cluster sizes. The absence of isomers is closely related to the fact that there are no ''magic'' cluster sizes of particular stability for the He_nHF series as has been found before for pure helium clusters.[1,70–72] The figure shows the density of helium in units of $Å^{-3}$ in cylinder coordinates r and z, averaged over

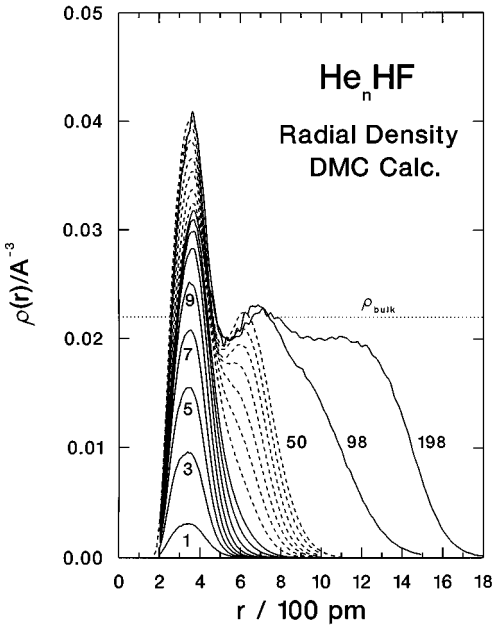

FIG. 8. Radial density distribution of He_nHF clusters, $n=1$, 3, 5, 7, 9, 11, 13, 15 (solid lines), 20, 25, 30, 35, 40, 45, 50 (dashed lines), and $n=98$ and 198. The dotted line indicates the density of bulk helium.

the azimuthal angle ϕ [see Eq. (25)]. The latter is possible because the Hamiltonian is anisotropic only with respect to θ and has rotational symmetry about the z-axis (see Sec. II C).

For all cluster sizes the density plot shows a very near spherical symmetry underlining the character of a quasi free HF rotor. There is a very small density increase on the hydrogen side of HF. Initially helium atoms are added in the immediate vicinity of HF such that the maximum density increases almost linearly without any shape change. After about 10 helium atoms have been attached to HF, build up of peripheral density starts while the density in the first maximum keeps growing slowly and eventually reaches twice the value of bulk helium of 0.022 $Å^{-3}$ (see Fig. 8).

This behavior coincides with the inflexion of the total energy curve in Fig. 6. Although the density profile and the trend for the total energies suggests an interpretation in terms of shells, the ongoing density increase in the nearest neighbor density maximum clearly shows that this structure has nothing to do with geometrical packing known from classical systems. The concept of shells becomes inappropriate for this type of cluster since also the density between the peaks remains very high and particles are exchanging positions between the inner and outer regions. This is a typical signature of a quantum liquid.

For the largest clusters one can nicely see a second ''shell'' with enhanced density and a plateau with a density very close to the bulk value of 0.022 $Å^{-3}$ and a diffuse edge where the density slowly drops to zero (see Fig. 2). The shape and thickness of this boundary region is in good agreement with calculations on pure helium clusters[42] and recent experimental results.[73] The largest cluster for which calculations were done (He_{198}HF) has a radius of about 20 Å .

The observation of almost perfectly isotropic cluster structures is surprising and leads to the interpretation of a free HF rotor which implies that the rotational spacings should be very similar to those observed in the free HF vibration–rotation spectrum. This is in contrast to SF_6 and Glyoxal embedded in helium clusters, where the rotational structure is two to three times denser than in the gas phase spectra.[11,12]

C. Excited HF

The total energies for He_nHF with vibrationally excited HF follow the same general trend as in the overall ground state. They are not shown separately in the graphical presentation of total energies (Fig. 6) because they coincide with the $v=0$ results within the size of the symbols. Also the density distributions are visually not discernible from those obtained in the respective ground states. VMC parameter optimizations were carried out separately for excited HF only for small clusters. The results of these calculations are collected in Table V.

More relevant for the comparison with the experiment is the HF vibrational frequency shift computed as a function of cluster size. For very small clusters the total energies are sufficiently accurate to allow direct energy difference estimates for the shift (column 4 in Table II) which agree well with the perturbational results in columns 5 and 6 which always have a significantly higher statistical accuracy. There is no statistically evident systematic difference between the energy difference estimates and the perturbational ones, the latter always falling inside the much larger error bar of the first. However, the comparison of the two perturbational estimates gives a feeling for the systematic error in this approach which is on the order of 5%.

Similar to the total energy, the vibrational redshift (see Fig. 9) grows approximately linear with cluster size for $n<10$ and again roughly linear with a much smaller slope up to about $n=50$. The redshift seems to saturate somewhere between $n=50$ and $n=100$. The value obtained for 198 helium atoms is statistically indistinguishable from the value at $n=100$ and gives us confidence that this asymptotic value of about -2.7 ± 0.1 cm^{-1} can be compared to the experimental value of -2.65 ± 0.15 cm^{-1} obtained for clusters with more than thousand atoms which are beyond the capabilities of the current method.

The observation of high symmetry in the helium density is relevant for the comparison of the computed HF frequency shift with the experimental value. The selection rules for optical transitions do not allow the rotationless transition whose energy is actually calculated in the theoretical treatment. The only observed line corresponds to the $R(0)$ transition on the blue side of the band center. The absence of other lines prevents the determination of the band center from a fit of rotational energy levels. This is due to the large separation of rotational levels in HF as opposed to SF_6 and Glyoxal, where several rotational transitions have been identified, allowing a unique determination of the band center[11,12]

TABLE IV. Wave function parameters and VMC energies for larger He_nHF clusters with HF in the $v = 0$ vibrational state described with wave function $\chi^{(3)}$ defined in Eq. (10). Dimensions of p_2, p_3, and p_4 depend on parameter values [see Eq. (10)]. The given values are appropriate for distances in a_0. Numbers in parentheses indicate uncertainties in units of the last digit.

n	p_0/a_0	p_1/a_0	p_2^a	p_3^a	p_4^a	E_0/cm^{-1}
10	5.50	6.750	0.95	0.95	−1.00	−71.52(3)
11	5.50	6.750	0.95	0.95	−1.00	−75.39(3)
12	5.50	6.750	0.95	0.95	−1.00	−77.34(3)
13	5.50	6.750	0.95	0.95	−1.00	−78.87(4)
14	5.50	6.750	0.92	0.91	−1.02	−81.39(5)
15	5.50	6.750	0.80	0.94	−1.00	−82.39(5)
16	5.50	6.705	0.90	0.85	−1.20	−84.70(5)
17	5.50	6.765	0.90	0.85	−1.50	−86.81(5)
18	5.50	6.745	0.90	0.83	−1.50	−88.47(5)
19	5.50	6.765	0.90	0.83	−1.50	−91.03(5)
20	5.50	6.765	0.90	0.83	−1.50	−92.94(5)
25	5.50	6.765	0.90	0.83	−1.50	−102.78(7)
30	5.50	6.765	0.90	0.83	−1.50	−112.73(9)
35	5.50	6.765	0.90	0.83	−1.50	−123.6(1)
40	5.50	6.765	0.90	0.83	−1.50	−129.2(2)
45	5.50	6.765	0.90	0.83	−1.50	−138.0(2)
50	5.50	6.765	0.90	0.83	−1.50	−143.2(2)

in spite of the very low cluster temperatures of only about 0.4 K.[11,75] The position of the $R(0)$ line is at about $\tilde{\nu}_0 + 2B_1$ in the gas phase spectrum, where B_1 is the rotational constant of HF in the $v = 1$ vibrational state (Table I). Centrifugal distortion plays a very minor role for this transition in HF. Since B_1 is 19.7875 cm^{-1},[52] already small changes in the effective rotational constant inside the liquid helium cluster would introduce significant uncertainties into the determination of the vibrational frequency shift. Only if the rotational structure is largely unperturbed is it legitimate to compare the redshift of the $R(0)$ transition with the theoretical value for the shift of the band center.

We assume that B_1 in the cluster is the same as in free HF on the basis of several observations: The density distribution of helium around HF becomes progressively isotropic with increasing cluster size but the anisotropy is already very small in the triatomic HeHF complex, where a noticeable contribution to the ground state energy arising from a hindered HF rotor was observed.[29] While the angular helium distribution provides rather circumstantial evidence for a free HF rotor, the latter observation can be turned into a quantitative instrument. If the rotor is hindered the ground state energy must be a function of the associated moment of inertia. In the free rotor limit there will be no contribution to the zero point energy and E_0 becomes independent of B_v.

We checked the dependence of the ground state energy of He_{20}HF on B_v by changing the latter by up to 25% in both directions but we could not find any effect on the zero point energy exceeding the DMC error bar of 0.15 cm^{-1} on the total energy. DVR-DGB test runs for the most anisotropic system, HeHF, resulted in an increase of the zero point energy by 0.0043 cm^{-1} if B_0 was increased by 1 cm^{-1} relative to its normal value of 20.5597 cm^{-1} and a lowering by 0.0047 cm^{-1} for a reduction of B_0 by 1 cm^{-1}. Similar tests of the energy sensitivity for Ar_2HF, which is known to have a significantly hindered HF rotor, resulted in changes exceeding the error bars of about 0.05 cm^{-1} by almost two orders of magnitude.[44] The anisotropy of the potential will be washed out with increasing cluster size. Even for the Ar_nHF and Ar_nHCl systems with a very anisotropic Ar–HX, X=F,Cl interaction the calculation of matrix shifts with isotropic free rotor models seems to work satisfactorily as soon as the nearest neighbor shell is completed.[74]

Inspection of the excited states of HeHF further supports the almost free rotor picture. The Σ and Π ''bending'' states of HeHF are energetically separated from the ground state by amounts that are close to $2B$ and the large splitting between the even and odd Π bend indicates very strong coupling to the overall rotation.

With this result we are in a position to convert the ex-

TABLE V. Wave function parameters and VMC energies for small He_nHF clusters with HF in the $v = 1$ vibrational state calculated with wave function $\chi^{(1)}$ defined in Eq. (8). Numbers in parentheses indicate uncertainties in units of the last digit.

n	p_0/a_0	p_1/a_0	p_2/a_0^{-1}	p_3	p_4	E_1/cm^{-1}
1	⋯	6.5039	0.6304	0.02165	−0.02003	−7.272(5)
2	6.0959	6.9035	0.8437	0.01667	−0.01643	−15.08(1)
3	5.6041	6.8010	0.8138	0.02026	−0.02142	−23.21(1)
4	5.4036	6.7973	0.8826	0.00617	−0.01498	−31.45(4)

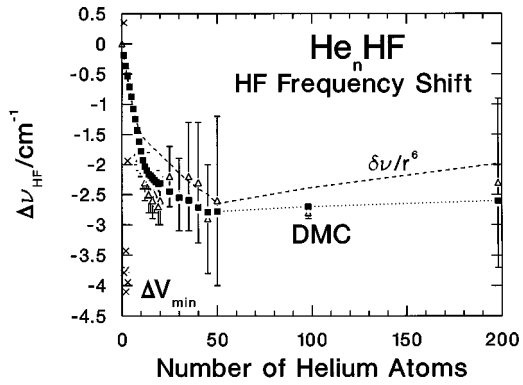

FIG. 9. Cluster size dependence of the HF frequency shift from DMC calculations, induction model, and potential minimization. Triangles with error bars are DMC energy difference estimates. Solid squares are DMC expectation values $\langle \Delta V \rangle_0$. $\langle \Delta V \rangle_1$ is slightly larger but not shown to avoid congestion. The dashed line shows the result of an integration of the DMC radial density distribution $\rho(r)$ [Eq. (24)] with a differential shift of $\delta\nu/r^6$ and $\delta\nu = -3100$ cm^{-1}Å^6. $\Delta V_{\min}$ (crosses) are estimates obtained by neglecting zero point energy effects and computing the difference between adiabatic potential minima.

perimentally observed $R(0)$ transition frequency into a value for the band center for comparison with the theoretical model. The experimental shift obtained in this way is -2.65 ± 0.15 cm^{-1} in very good agreement with the asymptotic DMC value of -2.7 ± 0.1 cm^{-1}. The VMC estimates for the frequency shift (Table II) are surprisingly good even though the total energies are in error by over 100 cm^{-1} for large clusters. This effect is clearly mainly due to error compensation but may be useful for calculations on even larger clusters where full DMC calculations are simply too costly.

In comparison to the profound effect of the helium cluster on the rotational structure of heavier molecules,[11,12] the occurrence of a free HF rotor first looks surprising. It does, however, make sense because the rotational spacings of SF_6 and Glyoxal are much smaller and lie significantly below the potential barriers towards internal rotation. These molecules are definitely turned into strongly hindered rotors for low rotational quantum numbers while for HF already the $J = 1$ state energetically exceeds the barrier in HeHF. The barrier towards internal rotation becomes very small once a first layer of helium is surrounding the HF molecule and smearing out this barrier.

The saturation of the shift somewhere between 50 and 100 helium atoms indicates that it clearly takes more than one neighbor shell to reach the bulk matrix limit. It is interesting to interpret the size dependence of the shift in terms of simple analytical models. The major mechanism invoked for the interpretation of vibrational shifts in large clusters is the dipole induced dipole interaction.[18,19,39] According to this model the shift should be dominated by the expectation value of the change of the induction energy upon excitation of the molecule. The induction energy can be simply calculated from known molecular properties according to

$$V^{\text{ind}} = -\frac{1}{2}\alpha |F|^2; \quad F = \frac{2\mu_v}{r^3}, \tag{35}$$

where α is the dipole polarizability of the rare gas and μ_v is the dipole moment of the diatomic in the vibrational state v.

As a first test we applied this model to HeHF using the known dipole moments of $\mu_0 = 1.827$ D and $\mu_1 = 1.874$ D for HF[76] and the polarizability of helium of $\alpha = 1.38\, a_0^3$.[77] The expectation value of $V_1^{\text{ind}} - V_0^{\text{ind}}$ was found to be -0.54 cm^{-1}, almost three times the exact value of -0.19 cm^{-1}. This is in contrast to the calculation for ArHF,[39] which gave -8.1 cm^{-1} to be compared to an observed shift of -9.65 cm^{-1}. In order to test if this model can at least reproduce the correct *trend* of the shift vs cluster size we performed calculations in which we assumed that each volume element of helium at a distance r from HF contributes a differential shift of $\delta\nu/r^6$ and integrated this term over the computed radial helium density distribution [Eq. (24)] in an isotropic approximation according to

$$\Delta\nu = 4\pi \int_0^\infty \delta\nu/r^6 \rho(r) r^2 dr. \tag{36}$$

The results from this model are indicated as a dashed line in Fig. 9 and qualitatively describe the size dependence of the computed vibrational shifts. The value of $\delta\nu$ was adjusted to -3100 cm^{-1}Å^6 to reproduce the DMC shifts calculated for small clusters. This leads to an underestimate of the asymptotic shift for large clusters by about 25%. This simple model also shows an earlier inflection of the incremental redshift. Inserting the values for μ and α appropriate for He and HF we obtain a prediction of -16300 cm^{-1} for $\delta\nu$ which clearly overestimates the redshift. Application of this method for frequency shift estimates for large clusters still requires knowledge of the radial density distribution which can currently only be obtained from large scale computations.

In order to quantify the quantum contribution to the frequency shift we performed minimizations of the adiabatic potential for several small clusters in both vibrational states of HF. If the zero point energy is identical in both adiabatic states the shift is simple given as the difference between these minimum energies. For Ar_nHF clusters this model was found to give the correct trend but to differ from the correct result by about a factor of two.[43,36] In the case of HeHF this model actually predicts a blue shift of 0.35 cm^{-1} for the linear He$\cdots$HF configuration and a redshift of -3.79 cm^{-1} for the He$\cdots$FH arrangement. For all isomers of He_2HF and He_3HF we obtained very strong redshifts between -2 and -7 cm^{-1}. These results are grossly incorrect and indicate the importance of the quantum mechanical averaging in this system. They are shown as little crosses in Fig. 9.

The excited vibrational state of HF in the helium cluster represents only a quasi bound state, since it couples to the helium bath and undergoes predissociation. This effect is at the heart of the experimental detection principle. The theoretical treatment is designed for strictly bound states but is applicable in this case since the leakage of energy from HF into the cluster is prevented by the adiabatic separation and the wave function is truly bound on the adiabatic surface. The finite lifetime provides one possible mechanism for the

experimentally observed broadening. The size distribution of the helium clusters should not contribute significantly to the linewidth since the calculation indicates that the frequency shift is constant within the observed linewidth for all clusters with more than about 100 atoms. Another broadening mechanism could be ''hot'' band transitions originating from excited phonon states of the helium cluster which might be thermally occupied even at the low cluster temperatures of about 0.4 K.[11,75] Combination band like excitation of the HF mode accompanied by phonon excitation may be possible but appears unlikely considering the observed gap in the vibronic spectrum of glyoxal in helium clusters.[12]

V. CONCLUSION

Considering the remaining uncertainty about the precise nature of the HF rotor and the simple pairwise additive potential model and the approximate adiabatic treatment, the good agreement between the predicted redshift and the actually observed value might in fact be somewhat fortuitous. In any case this result is encouraging and an impressive demonstration of the ability of quantum simulation methods to provide quantitative predictions for extended many particle systems. This success opens the way to study the helium matrix effect on more complicated molecules like water or ammonia, for which experimental information became very recently available.[62,78] We are working on further refinements of our computational procedures to increase the accuracy of the method still further and to eliminate remaining systematic errors.

An inverse adiabatic method which involves the solution of ground state problems for a series of fixed diatomic bond lengths for the construction of an effective diatomic potential function in the cluster environment has been applied recently for the computation of vibrational frequency shifts of N_2^+ in small helium clusters.[37] This approach more closely follows the original idea of Quack and Suhm[50] which was very successful for the calculation of the intermolecular stretching vibration in $(HF)_2$ but requires a large number of quantum simulations for each cluster size for the shift determination. We are planning to perform a study which compares the relative merits of these two available adiabatic methods.

ACKNOWLEDGMENTS

The assistance of R. Moszynski in resolving problems with the HeHF surface and in providing the original source code is gratefully acknowledged. M. L. thanks M. Mladenović for many inspiring discussions and help with the DVR-DGB calculations. We enjoyed fruitful discussions with M. Schinacher and the generous support of J. P. Toennies. F. H. and M. K. are thankful to the Deutsche Forschungsgemeinschaft (DFG) for a grant in the frame of its Schwerpunktsprogramm *Molekulare Cluster*. The IBM RS/6000-350 and DEC AXP3800 workstations and the DEC AlphaServer 2100 5/250 were purchased through Max Planck Society computing grants. The 4-processor SGI Power Challenge was made available by the Gesellschaft für Wissenschaftliche Datenverarbeitung Göttingen.

[1] V. R. Pandharipande, J. G. Zabolitzky, S. C. Pieper, R. B. Wiringa, and U. Helmbrecht, Phys. Rev. Lett. **50**, 1676 (1983); V. R. Pandharipande, S. C. Pieper, and R. B. Wiringa, Phys. Rev. B **34**, 4571 (1986).
[2] K. B. Whaley, Int. Rev. Phys. Chem. **13**, 41 (1994).
[3] S. A. Chin and E. Krotscheck, Phys. Rev. B **52**, 10405 (1995); E. Krotscheck and S. A. Chin, Chem. Phys. Lett. **227**, 143 (1994).
[4] D. M. Ceperley, Rev. Mod. Phys. **67**, 279 (1995).
[5] M. McMahon and K. B. Whaley, Chem. Phys. **182**, 119 (1994).
[6] A. Scheidemann, B. Schilling, and J. P. Toennies, J. Chem. Phys. **97**, 2128 (1993).
[7] M. Lewerenz, B. Schilling, and J. P. Toennies, Chem. Phys. Lett. **206**, 381 (1993).
[8] M. Lewerenz, B. Schilling, and J. P. Toennies, J. Chem. Phys. **102**, 8191 (1995).
[9] S. Goyal, D. L. Schutt, and G. Scoles, Phys. Rev. Lett. **69**, 933 (1992).
[10] F. Stienkemeier, J. Higgins, W. E. Ernst, and G. Scoles, Phys. Rev. Lett. **74**, 3592 (1995); Z. Phys. B **98**, 413 (1995); F. Stienkemeier, W. E. Ernst, J. Higgins, and G. Scoles, J. Chem. Phys. **102**, 615 (1995).
[11] R. Fröchtenicht, J. P. Toennies, and A. Vilesov, Chem. Phys. Lett. **229**, 1 (1994); M. Hartmann, R. E. Miller, J. P. Toennies, and A. Vilesov, Phys. Rev. Lett. **75**, 1566 (1995).
[12] M. Hartmann, F. Mielke, J. P. Toennies, A. Vilesov, and G. Benedek, Phys. Rev. Lett. **76**, 4560 (1996).
[13] C. M. Lovejoy and D. J. Nesbitt, J. Chem. Phys. **93**, 5387 (1990).
[14] J. I. Cline, B. P. Reid, D. D. Evard, N. Sivakumar, N. Halberstadt, and K. C. Janda, J. Chem. Phys. **89**, 3535 (1988); W. D. Sands, C. R. Bieler, and K. C. Janda, *ibid.* **95**, 729 (1991); D. G. Jahn, S. G. Clement, and K. C. Janda, *ibid.* **101**, 283 (1994).
[15] R. N. Barnett and K. B. Whaley, J. Chem. Phys. **96**, 2953 (1992); Z. Phys. D **31**, 75 (1994); M. A. McMahon, R. N. Barnett, and K. B. Whaley, J. Chem. Phys. **104**, 5080 (1996); M. A. McMahon and K. B. Whaley, *ibid.* **103**, 2561 (1995); Y. Kwon, D. M. Ceperley, and K. B. Whaley, *ibid.* **104**, 2341 (1996).
[16] F. Dalfovo, Z. Phys. D **14**, 263 (1989); **29**, 61 (1994).
[17] Z. Bačić, M. Kennedy-Mandziuk, J. W. Moskowitz, and K. E. Schmidt, J. Chem. Phys. **97**, 6472 (1992).
[18] R. N. Barnett and K. B. Whaley, J. Chem. Phys. **99**, 9730 (1993); **102**, 2290 (1995).
[19] D. Eichenauer and R. J. Le Roy, J. Chem. Phys. **88**, 2898 (1988).
[20] E. Cheng and K. B. Whaley, J. Chem. Phys. **104**, 3155 (1996).
[21] J. Jortner, Z. Phys. D **24**, 247 (1992); J. Chim. Phys. **92**, 205 (1995); J. Jortner and N. Ben-Horin, J. Chem. Phys. **98**, 9346 (1993); *Clusters of Atoms and Molecules I: Theory, Experiment, and Clusters of Atoms*, edited by H. Haberland (Springer, New York, 1994).
[22] W. Schöllkopf and J. P. Toennies, Science **266**, 1345 (1994); J. Chem. Phys. **104**, 1155 (1996).
[23] W. R. Rodwell, L. T. Sin Fai Lam, and R. O. Watts, Mol. Phys. **44**, 225 (1981).
[24] J. Tennyson and B. T. Sutcliffe, J. Chem. Phys. **79**, 43 (1983), and references therein.
[25] R. Moszynski, P. E. S. Wormer, B. Jeziorski, and A. van der Avoird, J. Chem. Phys. **101**, 2811 (1994); R. Moszynski (private communication).
[26] R. A. Aziz, F. R. W. McCourt, and C. C. K. Wong, Mol. Phys. **61**, 1487 (1987).
[27] K. T. Tang, J. P. Toennies, and C. L. Yiu, Phys. Rev. Lett. **74**, 1546 (1995).
[28] C. A. Parish and C. E. Dykstra, J. Chem. Phys. **98**, 437 (1993); A. Bhattacharya and J. B. Anderson, *ibid.* **100**, 8999 (1994).
[29] R. Moszynski, B. Jeziorski, A. van der Avoird, and P. E. S. Wormer, J. Chem. Phys. **101**, 2825 (1994).
[30] M. Mladenović (private communication).
[31] K. E. Schmidt and D. M. Ceperley, in *The Monte Carlo Method in Condensed Matter Physics*, Topics in Applied Physics Vol. 71, edited by K. Binder (Springer, New York, 1992); D. M. Ceperley and M. H. Kalos, in *Monte Carlo Methods in Statistical Physics*, Topics in Current Physics Vol. 7, edited by K. Binder (Springer, New York, 1986).
[32] D. M. Ceperley and B. Alder, Science **231**, 555 (1986); S. A. Chin, Phys. Rev. A **42**, 6991 (1990); M. A. Suhm and R. O. Watts, Phys. Rep. **204**, 293 (1991); W. A. Lester, Jr. and B. L. Hammond, Annu. Rev. Phys. Chem. **41**, 283 (1990).
[33] B. L. Hammond, W. A. Lester, Jr., and P. J. Reynolds, *Monte Carlo Methods in Ab Initio Quantum Chemistry* (World Scientific, Singapore, 1994).

[34] P. J. Reynolds, D. M. Ceperley, B. J. Alder, and W. A. Lester, Jr., J. Chem. Phys. **77**, 5593 (1982).
[35] C. J. Umrigar, M. P. Nightingale, and K. J. Runge, J. Chem. Phys. **99**, 2865 (1993).
[36] M. Lewerenz, J. Chem. Phys. **106**, 1028 (1996).
[37] D. F. R. Brown, J. Gregory, and D. C. Clary, J. Chem. Soc. Faraday Trans. **92**, 11 (1996).
[38] P. Niyaz, Z. Bačić, J. W. Moskowitz, and K. E. Schmidt, Chem. Phys. Lett. **252**, 23 (1996).
[39] J. M. Hutson, J. Phys. Chem. **96**, 4237 (1992); **96**, 6752 (1992); Annu. Rev. Phys. Chem. **41**, 123 (1990).
[40] M. H. Kalos and P. A. Whitlock, *Monte Carlo Methods* (Wiley, New York, 1986), Vol. 1; R. V. Rubinstein, *Simulation and the Monte Carlo Method* (Wiley, New York, 1981).
[41] N. Metropolis, A. W. Rosenbluth, M. N. Rosenbluth, A. H. Teller, and E. Teller, J. Chem. Phys. **21**, 1087 (1953).
[42] R. N. Barnett and K. B. Whaley, Phys. Rev. A **47**, 4082 (1993).
[43] S. Liu, Z. Bačić, J. W. Moskowitz, and K. E. Schmidt, J. Chem. Phys. **100**, 7166 (1994); S. Y. Liu, Z. Bačić, J. W. Moskowitz, and K. E. Schmidt, *ibid.* **101**, 6359, 10181 (1994).
[44] M. Lewerenz and M. Schinacher (unpublished).
[45] J. Wu and R. O. Watts (private communication).
[46] G. Hooß, Diploma thesis, University of Göttingen, 1994; G. Hooß and M. Lewerenz (unpublished).
[47] J. Anderson, J. Chem. Phys. **63**, 1499 (1975).
[48] D. Blume, M. Lewerenz, and M. Schinacher (unpublished).
[49] M. H. Kalos, J. Comp. Phys. **1**, 257 (1966); K. S. Liu, M. H. Kalos, and G. V. Chester, Phys. Rev. A **10**, 303 (1977); R. N. Barnett, P. J. Reynolds, and W. A. Lester, Jr., J. Chem. Phys. **96**, 2141 (1992); J. Comp. Phys. **96**, 258 (1991).
[50] M. Quack and M. A. Suhm, Chem. Phys. Lett. **183**, 187 (1991).
[51] V. Buch, J. Chem. Phys. **97**, 726 (1992).
[52] R. B. Le Blanc, J. B. White, and P. F. Bernath, J. Mol. Spectrosc. **164**, 574 (1994).
[53] B. H. Wells, Chem. Phys. Lett. **115**, 89 (1985); C. A. Traynor and J. B. Anderson, *ibid.* **147**, 389 (1988).
[54] J. W. Cooley, Math. Comput. **15**, 363 (1961); B. R. Johnson, J. Chem. Phys. **67**, 4086 (1977).
[55] J. N. Huffaker, J. Chem. Phys. **64**, 4564 (1976).
[56] A. M. Ferrenberg, D. P. Landau, and Y. J. Wong, Phys. Rev. Lett. **69**, 3382 (1992).
[57] I. Vattulainen, T. Ala-Nissila, and K. Kankaala, Phys. Rev. Lett. **73**, 2513 (1994); I. Vattulainen and T. Ala-Nissila, Comput. Phys. **9**, 500 (1995).
[58] S. Kirkpatrick and E. P. Stoll, J. Comp. Phys. **40**, 517 (1981).
[59] W. H. Press, B. P. Flannery, S. A. Teukolsky, and W. T. Vetterling, *Numerical Recipes in Fortran, 2nd ed.*, (Cambridge University Press, Cambridge, 1992).
[60] F. Huisken, M. Kaloudis, A. Kulcke, C. Laush, and J. M. Lisy, J. Chem. Phys. **103**, 5366 (1995).
[61] F. Huisken, M. Kaloudis, and A. Kulcke, J. Chem. Phys. **104**, 17 (1996).
[62] R. Fröchtenicht, M. Kaloudis, M. Koch, and F. Huisken, J. Chem. Phys. **105**, 6128 (1996).
[63] J. Harms (unpublished).
[64] F. Huisken, A. Kulcke, D. Voelkel, C. Laush, and J. M. Lisy, Appl. Phys. Lett. **62**, 805 (1993).
[65] HITRAN92 CD-data set, see J. Quant. Spectrosc. Radiat. Transfer **48**, 469 (1992).
[66] P. W. Anderson, Phys. Lett. A **29**, 563 (1968).
[67] M. Mladenović and Z. Bačić, J. Chem. Phys. **93**, 3039 (1991).
[68] M. Mladenović and M. Lewerenz (unpublished).
[69] B. T. Sutcliffe and J. Tennyson, Int. J. Quantum Chem. **39**, 183 (1991); J. Tennyson, S. Miller, and C. R. Le Sueur, Computer Phys. Commun. **51**, 73 (1988).
[70] R. Melzer and J. G. Zabolitzky, J. Phys. A: Math. Gen. **17**, L565 (1984).
[71] M. V. Rama Krishna and K. B. Whaley, J. Chem. Phys. **93**, 6738 (1990).
[72] S. W. Rick, D. L. Lynch, and J. D. Doll, J. Chem. Phys. **95**, 3506 (1991).
[73] F. Dalfovo, J. Harms, and J. P. Toennies (unpublished).
[74] B. Schmidt and P. Jungwirth, Chem. Phys. Lett. (to be published).
[75] D. M. Brink and S. Stringari, Z. Phys. D **15**, 257 (1990).
[76] S. M. Bass, R. L. DeLeon, and J. S. Muenter, J. Chem. Phys. **86**, 4305 (1987).
[77] K. T. Tang, J. M. Norbeck, and P. R. Certain, J. Chem. Phys. **64**, 3063 (1976).
[78] M. Behrens, U. Buck, R. Fröchtenicht, F. Huisken, and F. Rohmund (unpublished).